TRANSFORMATION IN IRON-ZINC ALLOYS

By

G. T. PARTHIBAN

DEPARTMENT OF METALLURGICAL ENGINEERING

DIAN INSTITUTE OF TECHNOLOGY KANPUR

AUGUST, 1983

TRANSFORMATION IN IRON-ZINC ALLOYS

A Thesis Submitted
in Partial Fulfilment of the Requirements
for the Degree of

MASTER OF TECHNOLOGY

By

G. T. PARTHIBAN

to the

DEPARTMENT OF METALLURGICAL ENGINEERING

INDIAN INSTITUTE OF TECHNOLOGY KANPUR

AUGUST, 1983

To my beloved sister

SREEMATHI PADHMA RAMAMOORTHY,

Whose love and will

made me what I am

this day.

ME-1983-M-PAR-TRA

CERTIFICATE

This is to certify that the work presented in this thesis entitled, "TRANSFORMATION IN IRON-ZINC ALLOYS", by G.T.Parthiban, has been carried out under my supervision and has not been submitted elsewhere for a degree.

August, 1983.

(S.P.Gupta)
Assistant Professor
Department of Metallurgical Engg.
Indian Institute of Technology
Kanpur

ACKNOWLEDGEMENTS

I am sincerely thankful to Dr.S.P.Gupta, for all the patient and understanding guidance he offered me, throughout this work.

I am thankful to Dr.K.P.Singh and Mr.M.N.Mungole, for their kind permission and assistance in using their laboratory.

My thanks are also due to Dr.M.N.Shetty and Dr.Jitendra Kumar for their assistance during the experimental part of this work.

I thank Mr.K.P.Mukherjee, D.Ramakrishna, V.P.Gupta, Deepak Goyal, Babu Viswanathan, Sukumar and U.S. Mishra for their assistance during photography, tracing and typing involved in this work.

I thank all my friends, who made my stay at IIT Kanpur a pleasant and memorable one.

-PARTHIBAN

CONTENTS

LIST OF FIGURES

LIST OF TABLES

ABSTRACT

The primary discontinuous precipitation and coarsening, were studied in Fe + 17.6 at. pct. Zn and Fe + 22.16 at. pct. Zn alloys, at different aging temperatures, ranging from 400°C to 520°C, using optical and scanning electron microscopy techniques. The reaction kinetics using the different models proposed and the morphology of the reaction were investigated, for both primary and secondary reactions.

Both primary and secondary cellular reactions are controlled by grain boundary diffusion of Zinc atoms. Among the different models investigated, Petermann-Hornbogen model is found to be the most suitable for both the reactions. This model considers the chemical free energy remaining after the primary reaction to be the driving force for the secondary reaction. Livingston and Cahn model on the other hand considers only the interfacial free energy difference between the primary and the secondary lamellae to be the driving force and is not appropriate because the interfacial free energy difference is two orders of magnitude less than the available chemical free energy.

The investigation on the morphology indicate that the primary precipitate nucleates at the grain-boundaries of supersaturated α - Fe and further growth occurs by the migration of this boundary. The moving primary cell-matrix interface leaves behind alternate lamellae of depleted α and

zinc rich Γ' phases. The secondary precipitate is observed to nucleate at original grain boundaries, at impinged regions of two primary cell-matrix interfaces, and at impinged regions of a primary cell interface and an original grain boundary. Further growth occurs by the migration of the nucleated boundary into the opposite grain (the grain opposite to that from which the secondary has nucleated). The secondary cell interface moves at a slower rate, leaving behind alternate lamellae of depleted α and Zinc rich Γ' phases, with larger interlamellar spacing, compared to that of the primary.

CHAPTER 1

INTRODUCTION

Although discontinuous coarsening or the secondary precipitation has been observed in many systems exhibiting cellular precipitation, only two theories have been developed to explain their growth kinetics. The first theory, by Livingston and Cahn (1), which is a modification of Zener's theory (2), proposes that the driving force for the secondary reaction is the decrease in the surface free-energy or the interfacial energy, accompanying the reaction. It however has its own shortcomings and does not account for the coarsening kinetics completely.

To overcome this, the second theory was developed by Fournelle (3), which is an extension of the theory of primary precipitation by Petemann and Hornbogen (4), based on Lucke's theory (5) of grain boundary migration. This theory considers the effect of chemical free-energy not used by primary precipitation, as a driving force.

To investigate the validity of these two theories, the kinetics of secondary precipitation in Fe + 17.6 at.pct. Zn and Fe + 22.16 at.pct. Zn alloys are analysed according to both the theories. Simultaneously, the kinetics of primary precipitation is analysed based on theories proposed by Turnbull (6), Aaronson 1(7), Aaronson 2(7), Cahn (8) and

Petermann and Hornbogen (4).

1.1 Iron-Zinc Phase Diagram:

The Fe + Zn equilibrium phase diagram is shown in Figure 1, after Speich, et.al. (9 and 10). The phase diagram shows a two phase ($\alpha + \Gamma$) region below the solvus and has the characteristic of increasing solid-solubility with decreasing temperature. The composition range suitable for precipitation reaction study, varies from 2.05 at. pct. Zn at 400°C to 42.12 at.pct Zn at 783°C. The compositions selected for this investigation, 17.6 at.pct. Zn and 22.16 at.pct. Zn, lie within this range. The solvus temperature for the 17.6 at.pct. Zn alloy is 632°C and that for the 22.16 at.pct. Zn alloy is 656°C, as estimated from the phase diagram, shown in Figure 1.

The alloys are solution treated at 700°C for 10 minutes to obtain a single phase, supersaturated α-Fe. They are immediately aged at different aging temperatures, ranging from 400°C to 520°C, when the Zn rich 'Γ' phase precipitates out. The precipitation reaction

$$\underset{\text{Supersat.}}{\alpha} \rightarrow \underset{\text{(BCC)}}{\alpha} + \underset{\text{(Complex-cubic)}}{\Gamma}$$

yields alternate lamellae of Fe-rich 'α' and Zn-rich 'Γ' phases.

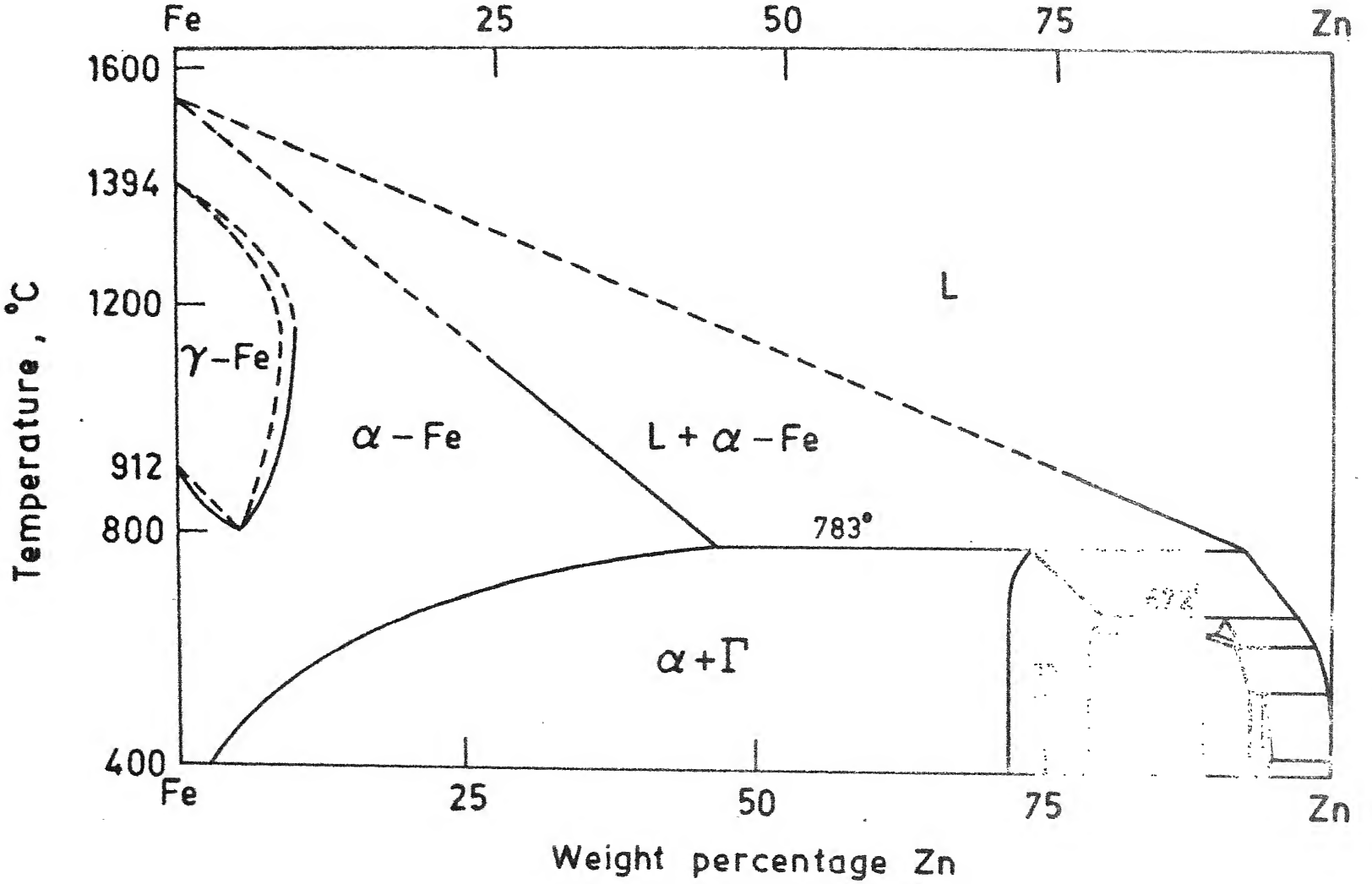

Fig. 1. The Iron-Zinc phase diagram.

1.2 Discontinuous Precipitation:

In a precipitation reaction, when the composition of the matrix changes abruptly or "discontinuously" along the reaction front, it is termed as 'Discontinuous Precipitation' (6,11-15). The original super-saturated solid solution of α-Fe is divided into an assembly of depleted-α and solute rich-Γ phases after the transformation. The transformed regions are called 'cells'. There are a number of alloy systems, where transformation by discontinuous mode is observed, eg., Al-Zn (15), Al-Ag (16), Au-Ni (17), Cr-Ni (18), Cu-In (13), Fe-Zn (9), Fe-Ni-Ti (14), Pb-Sn (12), etc.

In a cellular reaction, the cell boundary is the interface that separates the transformed and untransformed regions. The solute transfer occurs via the cell-boundary. The original solid solution of α-Fe and the lamellar product α are similar but for their solute content. The lamellar is solute depleted while the original solid solution of α-Fe is supersaturated with solute, So, the solute-rich Γ phase nucleates first, while the surrounding regions become the solute depleted-α.

Discontinuous precipitation preferentially starts at grain boundaries. Since grain boundaries lower the activation energy required for nucleation, formation of nuclei at grain boundary is preferred. The migration of the nucleated boundary results in the formation of cellular structures, exhibiting

alternate lamellae of depleted- α and solute rich Γ phases.

1.2.1 Mechanism of Discontinuous Precipitation:

According to Smith (19), solute segregates from a supersaturated solid solution by discontinuous precipitation when the boundary between two adjacent supersaturated grains becomes unstable and migrates into the opposite grain. As the boundary migrates, an aggregate of the precipitate phase and depleted solid solution is formed behind the advancing interface. This aggregate is characterised by a regular arrangement of the precipitate and the depleted matrix phase, having the same orientation as the grain from which it grew. The driving force for discontinuous precipitation is the decrease in the chemical free energy, accompanying the reaction. Segregation of excess solute occurs in the advancing cell interface by boundary rather than in front of it by volume diffusion, according to Tu, et.al. (20). The only requirement the interface must meet is that it has to be a high angle boundary, so that it is suitable for mass transport and is highly mobile. It also provides many heterogeneous nucleation sites. The thermodynamic stimulus for the migration of the nucleated boundary is the difference between the volume free energy of the initial supersaturated solid solution and that of the transformed products within the cells.

Boundary Migration during Discontinuous Precipitation:

In the temperature range of discontinuous precipitation, the volume diffusivity of the solute is very low in many systems exhibiting the above transformation. The transformation, however, is observed at measurable rates. The nucleation problem is overcome by the boundary diffusion of solute. Continued growth of the precipitate will require a steady supply of solute to the boundary. If the boundary is immobile, the solute must come to the boundary through long range volume diffusion. This is not possible, as the volume diffusivity is very low. Therefore, for continued growth of the precipitate, the boundary must migrate and so the cell growth is boundary diffusion controlled.

In consideration to the heterogeneous nucleation, it has been observed that a heterogenity like a grain boundary remains stationary on nucleation. Therefore, a process must evolve, which mobilizes the boundary, since discontinuous precipitation requires continued migration of the cell boundary.

Consider the precipitate formed to be shaped like a hemispherical cap, along the grain boundary (a grain boundary allotriomorph). Under the influence of the surface tension of the α/γ interface, the nucleus does not exert a force or a torque on the boundary and so, the boundary remains stationary.

Now, consider the precipitate in the shape of a thin disc. When the precipitate maintains a habit with the matrix (i.e. certain plane and direction of the precipitate matches with a certain plane and direction of the matrix, respectively) on one side of the grain boundary and lies in the plane of the boundary, it satisfies a number of requirements:

1) The activation energy for nucleation is lowered, when nuclei of the precipitate lie in the plane of the grain boundary.
2) The average interfacial energy of the α/Γ interface will be lower than that when the precipitate maintains arbitrary orientation relationship with both the grains.
3) In order to maintain a habit plane, a torque must be applied, so that the grain boundary gets twisted locally. This sets the grain boundary in motion.

Once the grain boundary is in motion, it can further reduce the interfacial energy if both broad faces of the precipitate lie within the same grain with lower interfacial energy. This is achieved by the migration of the boundary along broad faces of the precipitate.

1.3 Theories on Cellular Precipitation:

1.3.1 Turnbull's Theory (6):

The number of solute atoms, leaving the supersaturated α -phase, assuming steady state, is given by solving Fick's Ist law, as,

$$\frac{dm}{dt} = \frac{A^{\alpha} D_B}{V_m} \cdot \frac{dX_B}{dy} \qquad (1)$$

where,

A^{α} = Area of α -phase, from which the solute atoms leave

D_B = Boundary diffusivity of solute atoms

$\frac{dX_B}{dy}$ = Concentration gradient

V_m = Molar volume of the alloy.

If 'δ' is the boundary thickness and 'b' is distance parameter perpendicular to growth direction, then,

$$A^{\alpha} = b\,\delta \qquad (2)$$

Also, the effective diffusion distance was assumed to be S^{α} (i.e.)

$$dy = S^{\alpha} = S - S_{\Gamma} \qquad (3)$$

where,

S^{α} = Width of α -lamellae

S^{Γ} = Width of Γ -lamellae

S = Interlammellar spacing = $S^{\alpha} + S^{\Gamma}$

Since the α and Γ phases grow together during discontinuous precipitation, the width of individual lamellae are given by Lever's Principle as

$$\frac{S^{\alpha}}{V_m} = \left[\frac{X_B^{\Gamma} - {}^1X_B^{\alpha}}{X_B^{\Gamma} - X_B^{\alpha}} \cdot \frac{1}{V_m} \right] S \qquad (4)$$

$$\frac{S^{\Gamma}}{V_m} = \left[\frac{{}^1X_B^{\alpha} - X_B^{\alpha}}{X_B^{\Gamma} - X_B^{\alpha}} \cdot \frac{1}{V_m} \right] S \qquad (5)$$

where,

X_B^{Γ} = Mole fraction of solute in Γ phase

X_B^{α} = Mole fraction of solute in α phase

${}^1X_B^{\alpha}$ = Mole fraction of solute in the supersaturated solid solution of original alloy

If v is the growth velocity, then,

$$\frac{dm}{dt} = v\, b \frac{S^{\alpha}}{V_m} ({}^1X_B^{\alpha} - X_B^{\alpha}) = v\, b \frac{S^{\Gamma}}{V_m} (X_B^{\Gamma} - {}^1X_B^{\alpha}) \qquad (6)$$

Substituting (2) and (3) in (1), then combining with (6), and rearranging, we have,

$$v = \frac{D_B \delta \cdot \Delta X_B}{(S^{\alpha})^2 ({}^1X_B^{\alpha} - X_B^{\alpha})} \qquad (7)$$

Turnbull neglected the effect of surface energies in the driving force for diffusion and approximated,

$$\Delta X_B = {}^1X_B^{\alpha} - {}^eX_B^{\alpha/\Gamma} \qquad (8)$$

and also neglected X_B^{α} in comparison with ${}^1X_B^{\alpha}$ (9)

(8) and (9), when used in (7), lead to

$$v = \frac{D_B \delta}{S^2} \cdot \frac{({}^1X_B^{\alpha} - {}^eX_B^{\alpha/\Gamma})}{{}^1X_B^{\alpha}} \qquad (10)$$

1.3.2 Aaronson and Liu Treatment (7):

Turnbull's treatment was modified by Aaronson and Liu as:

(1) X_B^{α} can not be neglected with respect to ${}^1X_B^{\alpha}$ and that

$$X_B^{\alpha} = {}^eX_B^{\alpha/\Gamma} \qquad (11)$$

(2) $A^{\alpha} = 2\,b\,\delta$ (12)

since solute atoms leave an α-lamelle in both directions.

Retaining Zener's assumption (2) that $dy = \frac{S}{2}$, substituting (11) and (12) in (1), and solving, they showed,

$$v = \frac{4\,D_B\,\delta}{S^2}\left[\frac{X_B^{\Gamma} - X_B^{\alpha}}{X_B^{\Gamma} - {}^1X_B^{\alpha}}\right] \qquad (13)$$

Later, equation (13) was further modified by Aaronson and Liu (7), approximating ${}^1X_B^{\alpha} = X_B^{\alpha}$, to give

$$v = \frac{4\,D_B\,\delta}{S^2}\left[\frac{X_B^{\Gamma} - X_B^{\alpha}}{X_B^{\Gamma} - X_B^{\alpha}}\right]\left[\frac{X_B^{\alpha} - {}^eX_B^{\alpha/\Gamma}}{X_B^{\alpha} - X_B^{\alpha}}\right] \qquad (14)$$

1.3.3 Cahn's Treatment (8):

The diffusion equation for cellular growth, given by Cahn is,

$$D_B^B \delta \frac{d^2 X_B^B}{dz^2} + v \left({}^1X_B^{\alpha} - X_B^{\alpha} \right) = 0 \qquad (15)$$

where it is assumed that:

(1) grain boundary diffusion is the only operative mass transport process

(2) the boundary can be represented by a thickness 'δ', and concentration X_{Zn}^B, with a constant diffusion coefficient D_{Zn}^B

(3) the system is at steady-state

and (4) the cell boundary is planar

Suffix B ⟶ solute (Zn) ; Prefix B ⟶ boundary

v = growth velocity or boundary migration rate

z = distance along boundary, measured normal to lamellae.

Cahn also assumed that, $\frac{X_B^{\alpha}}{X_B^B} = k = \text{constant}, \qquad (16)$

equilibrium exists at α/Γ interfaces and that Γ lamellae are thin with respect to S (interlamellar spacing), so that the boundary conditions are:

$$X_B^{\alpha} = {}^eX_B^{\alpha} \text{ at } Z = \pm \frac{S}{2}.$$

The solution to (15) is then,

$$\frac{X_B^{\alpha} - {}^{1}X_B^{\alpha}}{{}^{e}X_B^{\alpha} - {}^{1}X_B^{\alpha}} = \frac{\text{Cos h } (\frac{z}{s}\sqrt{A})}{\text{Cos h } (\frac{1}{2}\sqrt{A})} \tag{17}$$

where,

$$A = \frac{k\, v\, s^2}{D_B^B\, \delta} \tag{18}$$

Cahn has approximated the chemical free-energy change for non-equilibrium segregation as,

$$\Delta F_c = -\left[RT \left({}^{1}X_B^{\alpha} \ln \frac{{}^{1}X_B^{\alpha}}{{}^{e}X_B^{\alpha}} + {}^{1}X_A^{\alpha} \ln \frac{{}^{1}X_A^{\alpha}}{{}^{e}X_A^{\alpha}} \right) \right] \left[1 - \left(\frac{X_B^{\alpha} - {}^{e}X_B^{\alpha}}{{}^{1}X_B^{\alpha} - {}^{e}X_B^{\alpha}} \right)^2 \right] \tag{19}$$

The fraction P of the chemical free-energy for equilibrium segregation actually released by cellular precipitation can be obtained by integrating ΔF_c (equation (19)), over the entire cell. Substituting for X_B^{α} from equation (17) in equation (19) and integrating, we have,

$$P = \frac{3}{\sqrt{A}} \text{ tan h } (\tfrac{1}{2}\sqrt{A}) - \tfrac{1}{2} \text{ sec h}^2 (\sqrt{A}) \tag{20}$$

Cahn has also evaluated the fraction of solute used during cellular precipitation as,

$$W = \frac{2}{\sqrt{A}} \text{ tan h } \frac{\sqrt{A}}{2} \tag{21}$$

where 'W' can be experimentally evaluated and hence A could be calculated.

1.3.4 Petermann and Hornbogen's Theory (4):

According to Petermann and Hornbogen, the growth velocity is given by,

$$v = - M . \Delta G \qquad (22)$$

where,

M = grain boundary mobility

ΔG = driving force for the growth of cells.

The mobility is a function of temperature (T) and is determined from the atomic jump frequency $\frac{1}{\tau}$ (τ = period of jump) and the grain boundary thickness, 'δ'. For the cell boundary to migrate, the solute atoms have to diffuse a distance = $\frac{S}{2}$, to the γ' -phase. Time taken by the solute atoms to move a distance = $\frac{S}{2}$ is given by,

$$(\frac{S}{2})^2 = 2 D_B \tau \qquad (23)$$

Therefore,

$$\tau = \frac{S^2}{8 D_B} \qquad (24)$$

Substituting (24) in (22), we get,

$$v = - \frac{8 D_B \delta}{RT S^2} \Delta G \qquad (25)$$

The amount of chemical free energy available to drive the reaction can be estimated with the help of free-energy vs composition diagram:

$$\Delta G = f \Delta G_o + \frac{2 \gamma V_m}{S} \qquad (26)$$

where,

γ = specific surface energy of α/γ interface

f = fraction of ΔG_o (chemical free energy) released during the reaction.

$$\Delta G = RT \left[{}^{1}X_B^{\alpha} \ln \frac{X_B^{\alpha}}{{}^{1}X_B^{\alpha}} + {}^{1}X_A^{\alpha} \ln \frac{X_A^{\alpha}}{{}^{1}X_A^{\alpha}} \right] + \frac{2 \gamma V_m}{S} \qquad (27)$$

Combining (25) and (27), the equation for the growth velocity is written as,

$$v = - \frac{8 D_B \delta}{S^2 RT} \left[RT \left\{ {}^{1}X_B^{\alpha} \ln \frac{X_B^{\alpha}}{{}^{1}X_B^{\alpha}} + {}^{1}X_A^{\alpha} \ln \frac{X_A^{\alpha}}{{}^{1}X_A^{\alpha}} \right\} + \frac{2 \gamma V_m}{S} \right] \qquad (28)$$

1.4 Discontinuous Coarsening or 'Secondary Precipitation':

When the discontinuously precipitating systems were aged for longer periods of time at their respective aging temperatures, they were found to coarsen, resulting into products as in the primary precipitate (1,4,21,22,23). This coarsening of discontinuous precipitates, is observed to decompose the products of the primary cellular reactions. The primary dissolves just ahead of the coarsening cell-boundary. As in the primary precipitation, this second cell-boundary also migrates, leaving behind phases with larger inter-lamellar spacing and a larger volume fraction

of the precipitated phase. The solute is redistributed at this second cell boundary, resulting in the growth of secondary cells 'or'secondary precipitate' at a slower rate and a larger inter-lamellar spacing as compared to the primary.

These secondary cells are observed to originate, prior to the completion of the primary transformation, at all aging temperatures. They are observed to nucleate preferentially at the original grain boundaries of the parent matrix, at primary cell intersections, and at the intersection of the original grain boundary and a primary cell boundary. The migration of the nucleated boundary, into the opposite grain, results in the growth of secondary precipitate.

Theories for the Discontinuous Coarsening of Cellular Precipitate:

1.4.1 Livingston and Cahn's Theory (1):

According to the model proposed by Livingston and Cahn, the driving force for the coarsening of cells is the reduction in the free energy accompanying the formation of secondary cells from the primary cells, given by,

$$-\Delta G = 2\gamma V_m\left[\frac{1}{S_1} - \frac{1}{S_2}\right] \qquad (29)$$

Where:

S_1 and S_2 are interlamellar spacings of primary and secondary cells respectively.

Since the transformation of secondary cells from the primary cells also occurs by grain boundary migration, with the solute driven down the concentrated gradient built-up at the grain boundary, the release of an amount of energy, ΔG, is converted to drive the grain boundary concentration gradient through the Gibbs-Thompson effect at the tip of the second cell lamellae.

Considering steady-state, the rate of mass transport through the cell boundary in front of the α lamellae, from Fick's Ist law is,

$$\frac{dm}{dt} = D_B \cdot 2b\delta \frac{\Delta X_B}{(S_2^{\alpha}/2)} \qquad (30)$$

where,

ΔX_B = the concentration difference arising out of the Gibbs-Thompson effect

$$= \frac{2\gamma V_m}{S_1}\left[1 - \frac{S_1}{S_2}\right] {}_B X_B^{\alpha} \qquad (31)$$

and $\frac{S_2^{\alpha}}{2}$ = effective diffusion distance, using Zenar's approximation.

The matter transported in front of the α-lamellae helps grow the Γ phase of secondary cells and therefore, the rate of mass transport in front of Γ lamellae must equal

the same in front of α lamellae.

The rate of mass transport in front of Γ lamellae is,

$$\frac{dm}{dt} = V\, b\, S_2^{\Gamma} (X_B^{\Gamma} - {}^1X_B^{\alpha}) \tag{32}$$

So,

$$V\, b\, S_2^{\Gamma} (X_B^{\Gamma} - {}^1X_B^{\alpha}) = 8\, D_B\, b \frac{\delta \gamma V_m}{S_2^{\alpha}\, RT} \frac{1}{S_1}\left[1 - \frac{S_1}{S_2}\right] B X_B^{\alpha} \tag{33}$$

since,

$$\frac{dm}{dt} = \frac{Vb}{V_m} S_2^{\alpha} ({}^1X_B^{\alpha} - X_B^{\alpha}) = \frac{Vb}{V_m} S_2^{\Gamma} (X_B^{\Gamma} - {}^1X_B^{\alpha})$$

$$= V\, S_2\, b\, f_2^{\alpha} f_2^{\Gamma} (X_B^{\Gamma} - X_B^{\alpha}) \tag{34}$$

Therefore,

$$V = \frac{8\, D_B\, \delta}{(f_2^{\alpha})^2 (f_2^{\Gamma})^2} \cdot \frac{(X_B^{\Gamma} - {}^1X_B^{\alpha})}{(X_B^{\Gamma} - X_B^{\alpha})^2} \cdot \frac{({}^1X_B^{\alpha} - X_B^{\alpha})}{(X_B^{\Gamma} - {}^1X_B^{\alpha})} \frac{V_m \gamma {}^B X_B^{\alpha}}{S_2^2\, S_1 RT}\left[1 - \frac{S_1}{S_2}\right]$$

$$= \frac{8\, D_B\, \delta}{(f_2^{\alpha})^2 (f_2^{\Gamma})} \frac{B X_B^{\alpha}}{(X_B^{\Gamma} - X_B^{\alpha})} \cdot \frac{\gamma V_m}{S_2^2\, S_1 RT}\left[1 - \frac{S_1}{S_2}\right] \tag{35}$$

The same equation can be arrived at by considering the rate of mass transport in front of an α-lamellae, which is,

$$\frac{dm}{dt} = \frac{Vb}{V_m} S_2^{\alpha} ({}^1X_B^{\alpha} - X_B^{\alpha})$$

and upon equating the rate of mass transport from the two

sources gives,

$$V = \frac{8 D_B \delta}{(f_2^{\alpha})^2 (f_2^{\Gamma})^2} \cdot \frac{({}^1X_B^{\alpha} - X_B^{\alpha})^2 \cdot {}^BX_B^{\alpha}}{(X_B^{\Gamma} - X_B^{\alpha})^2 ({}^1X_B^{\alpha} - X_B^{\alpha})} \cdot \frac{\gamma V_m}{S_2^2 S_1 RT} \left[1 - \frac{S_1}{S_2} \right]$$

$$V = \frac{8 D_B \delta}{(f_2^{\alpha})^2 (f_2^{\Gamma})} \cdot \frac{{}^BX_B^{\alpha}}{(X_B^{\Gamma} - X_B^{\alpha})} \cdot \frac{\gamma V_m}{S_2^2 S_1 RT} \left[1 - \frac{S_1}{S_2} \right] \qquad (36)$$

1.4.2 Petermann and Hornbogen's Theory (4):

As shown earlier, the growth velocity of the primary cells during cellular phase transformation is,

$$V_1 = - \frac{8 D_B \delta}{RT \; S_1^2} \Delta G \qquad (37)$$

The chemical free energy, ΔG, available to drive the reaction is,

$$\Delta G = f \Delta G_o + \frac{2 \gamma V_m}{S_1} \qquad (38)$$

where,

f. ΔG_o = fraction of total chemical free energy, ΔG_o, available to drive the reaction to primary cells, a part of which $\frac{2 \gamma V_m}{S_1}$ (+) goes to the newly created α/Γ interface.

Therefore,

$$v_1 = - \frac{8 D_B \delta}{RT S_1^2} \left[f \Delta G_o + \frac{2 \gamma V_m}{S_1} \right] \qquad (39)$$

If it is assumed that during the growth of the secondary cells, the remaining free energy is used, because it grows considerably slowly as compared to primary cells, then,

$$\Delta G_2 = (1-f) \Delta G_o - \left(\frac{2 \gamma V_m}{S_1} - \frac{2 \gamma V_m}{S_2} \right) \qquad (40)$$

Assuming that the second cell growth follows the Petermann and Hornbogen's growth kinetics, then,

$$v_2 = - \frac{8 D_B \delta}{S_2^2 RT} \left[(1-f) \Delta G_o - 2 \gamma V_m \left(\frac{1}{S_1} - \frac{1}{S_2} \right) \right] \qquad (41)$$

The only unknown quantity, which can not be experimentally determined is the fraction of the available free energy to drive the reaction, until and unless, the exact shape of the G_m^{α} and G_m^{Γ} curves are known. Thus by solving for f. ΔG_o equation (38) gives,

$$f. \Delta G_o = - \frac{RT S_1^2 V_1}{8 D_B \delta} - \frac{2 \gamma V_m}{S_1} \qquad (42)$$

Substituting for f. ΔG_o from (42), in equation (41) one obtains,

$$v_2 = - \frac{8 D_B \delta}{S_2^2 RT} \left[\Delta G_o + \frac{RT S_1^2 v_1}{8 D_B \delta} + \frac{2 \gamma V_m}{S_1} - \frac{2 \gamma V_m}{S_1} + \frac{2 \gamma V_m}{S_2} \right]$$

i.e.,

$$v_2 = - \frac{8 D_B \delta}{S_2^2 RT} \left[\Delta G_o + \frac{2 \gamma V_m}{S_2} \right] - \frac{S_1^2}{S_2^2} v_1 \qquad (43)$$

CHAPTER 2

EXPERIMENTAL PROCEDURE

2.1 Alloy Preparation:

Alloys for this investigation were prepared by using 99.999% pure Zinc and Iron. Iron sheets with weighed amount of well cleaned Zinc were encapsulated in quartz tubes after holding them under vacuum of 10^{-5} torr or better. In order to avoid contact between Iron and Zinc, which otherwise would have led to the formation of Zinc-rich alloy locally, Iron sheet and Zinc pieces were separated from each other by a necked region in the quartz tube.

These encapsulated quartz tubes were placed in a horizontal tubular furnace for vapour deposition of Zinc over Iron. For the preparation of the alloy, the starting furnace temperature was 600°C. After keeping the quartz tubes at 600°C for one week, the furnace temperature was maintained at 700°C, 800°C, and 900°C for two weeks at each temperature, followed by three weeks at 950°C. During this process, the diffusion of Zinc into Iron occurred and thus the alloy was formed. After the final homogenization at 950°C, the alloy was quenched in a mixture of ice and water. A number of such alloys were made.

2.2 Heat-treatment of the alloy:

Specimens for the kinetic study were cut from prepared alloys. These were encapsulated in quartz tubes after holding them under vacuum of about 10^{-3} torr, to avoid oxidation.

The encapsulated specimen was solution-treated at 700°C, for 10 minutes, and immediately aged, for different times. The temperatures of aging ranged from 400°C to 520°C. The times of aging were selected according to the temperature. The specimen was quenched, in a mixture of ice and water, after aging.

2.3 Examination of treated specimens:

The heat-treated specimens were polished on different grades of emery paper and then finally polished on polishing cloth with alumina powder. The polished specimens were washed in water and etched with a solution of 3% nital.

2.3.1 Optical Microscopic Examination:

The growth rate and inter-lamellar spacing, were measured with the help of the optical microscope, for both primary and secondary precipitates.

The growth rate at each temperature, was determined by measuring the width of precipitate, at each time of aging. An average of 25 such measurements was taken as the growth distance, for growth rate calculations.

The least square method was used to calculate the growth rate.

The interlamellar spacing at each temperature was determined by measuring the number of lamellae, present within a specific distance. 30 such readings were taken per sample, and averaged.

2.3.2 Scanning Electron Microscope Examination:

The inter-lamellar spacing and degree of segregation were measured using scanning electron microscope. In order to resolve the lamellae, sufficiently high magnification was used both for primary and secondary precipitates. The lamellar structure was recorded on a photograph and the measurements were made to determine the interlamellar spacing.

The interlamellar spacing was measured by counting the number of lamellae within a specific distance. Several such readings were taken for each sample and an average was taken to get the interlamellar spacing at each temperature.

The samples were examined with SEM mainly to estimate the degree of segregation (i.e.) the solute content of the depleted α , in equilibrium with the precipitated β phase. The width of β lamellae (L^{β}) was measured within a specific distance (L). The ratio between L^{β} and L gives the volume fraction of the β phase, formed at that aging temperature. The Zn content of the β phase was taken to be 70 atomic percent (i.e.) $X_{Zn}^{\beta} = 0.7$. By substituting the volume fraction

of Γ and X_{Zn}^{Γ} in the equation [GR Speich, (9)] ,

$$X_{Zn}^{\alpha} = {}^{1}X_{Zn}^{\alpha} - (X_{Zn}^{\Gamma} - {}^{1}X_{Zn}^{\alpha}) \frac{V_m^{alloy}}{V_m^{\Gamma}} \cdot \frac{f}{1 - f} \qquad (44)$$

the degree of segregation can be evaluated, where,

X_{Zn}^{α} = Zn content of depleted-α in equilibrium with Γ
(i.e.) degree of segregation

${}^{1}X_{Zn}^{\alpha}$ = Zn content of the original alloy.

V_m^{alloy} and V_m^{Γ} = molar volumes of the alloy and Γ phase respectively (calculated from their lattice parameters)

f = volume fraction of the Γ phase.

CHAPTER 3

RESULTS

The following parameters were measured to analyse the kinetics of primary and secondary precipitation:

1. Growth Rate
2. Inter-lamellar Spacing
3. Degree of Segregation

3.1 Growth Rate (v):

Figures 2 and 3 show the growth distance vs. time plots for primary and secondary precipitation, respectively measured for a 17.6 at. pct. Zn alloy. It is observed that the growth distance increases linearly with time at each temperature. The growth rates were measured by least square method and are given in Table 1. Similar behaviour was observed for the 22.16 at. pct. Zn alloy and the growth rates are also given in Table 1.

The primary growth rates are found to be of the order of 10^{-9}m/sec and that of the secondary are 10^{-11}m/sec, for both the alloys. The growth rates of 22.16 at. pct. Zn alloy are relatively higher than that of the 17.6 at.pct. Zn alloy, both during primary and secondary precipitation, as shown in the growth rate vs. ΔT ($\Delta T = T_s - T_a$, where T_s = solvus temperature of the alloy and T_a = aging temperature) plot, given in Figure 4. The growth rate vs. ΔT plot indicates a

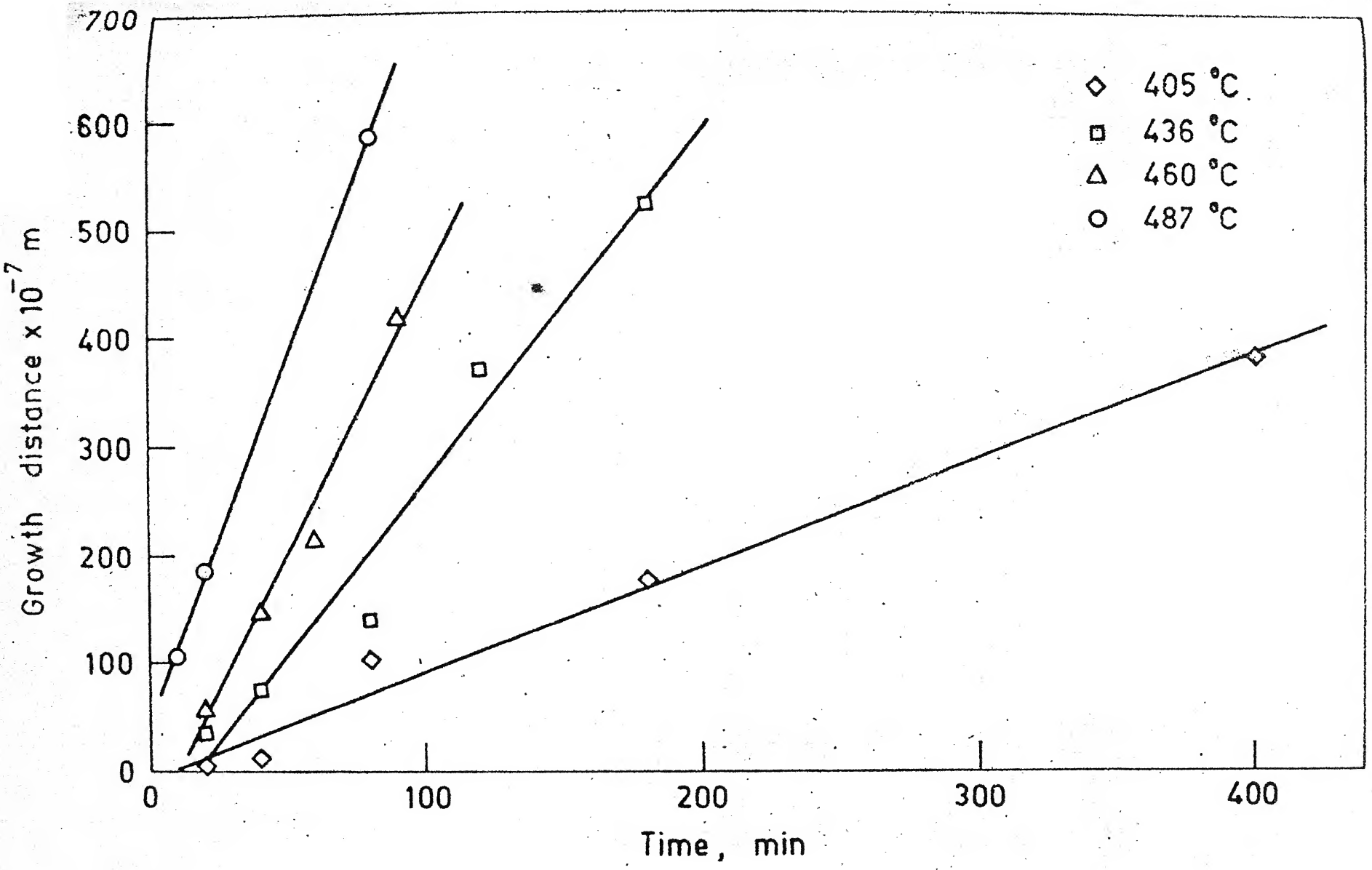

Fig. 2. Time vs growth distance for Fe + 17.6 at. % Zn, Primary.

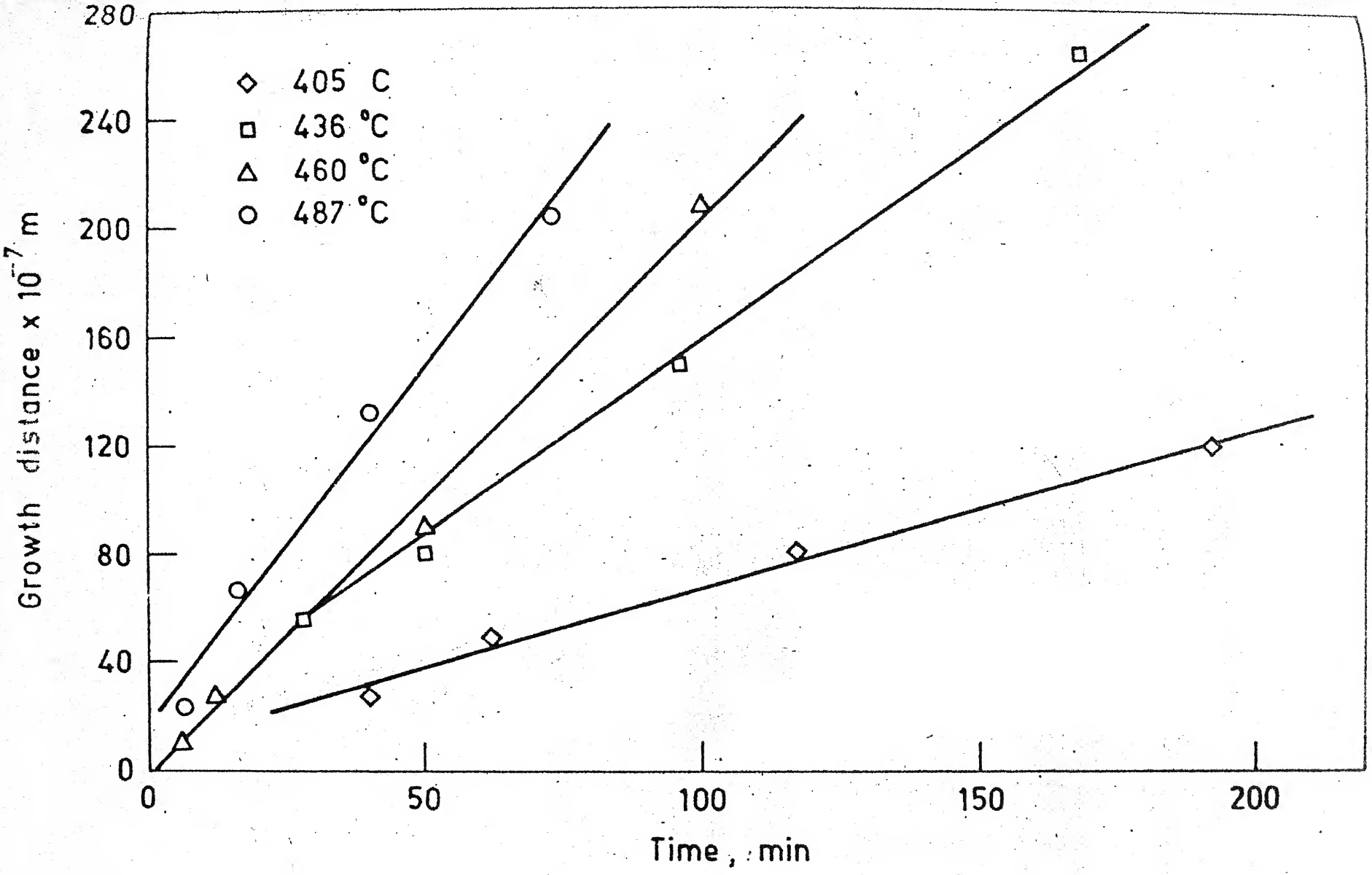

Fig. 3. Time vs growth distance for Fe + 17.6 at. % Zn, Secondary.

TABLE 1 : TEMPERATURE-GROWTH VELOCITY DATA FOR BOTH ALLOY

Alloy	Temperature (°C)	Growth Velocity	
		Primary $v_1 \times 10^9$ m/sec	Secondary $v_2 \times 10^{11}$ m/sec
17.6 at.pct.Zn	487	11.3178	7.353
	460	8.5	5.7363
	436	5.3625	3.9852
	405	1.6566	1.6492
22.16 at.pct.Zn	520	22.8	26
	490	29.5	33.8
	460	13.8	23
	420	6.4	7.2
	400	2.82	2.7

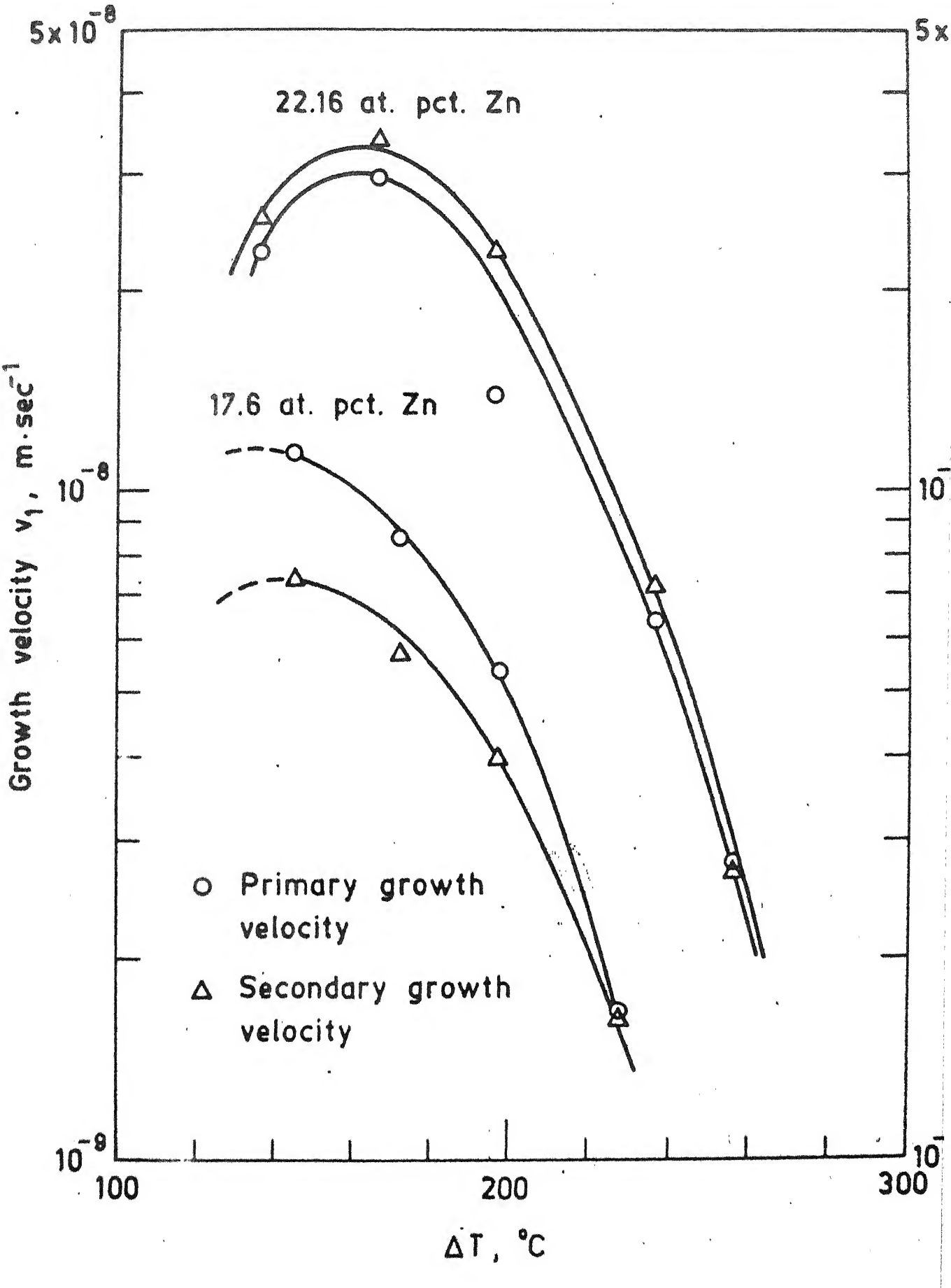
5x10⁻⁸
5x
22.16 at. pct. Zn
17.6 at. pct. Zn
10⁻⁸
10⁻
10⁻⁹
10⁻
Growth velocity v₁, m·sec⁻¹
○ Primary growth velocity
△ Secondary growth velocity
100
200
300
ΔT, °C

maximum growth velocity close to 490°C, for both primary and secondary precipitates within experimental error. As Δ T increases, both primary and secondary growth velocities (v_1 and v_2 respectively) are found to increase upto the Δ T corresponding to T_a = 490°C and steeply decrease at lower temperatures. This is observed in both alloys.

3.2 Inter-lamellar Spacing (S):

The inter-lamellar spacings, measured at different aging temperatures, for both the alloys are given in Table 2. Both primary and secondary inter-lamellar spacings are of the order of 10^{-7}m. It is observed that the 17.6 at. pct. Zn alloy shows a higher primary inter-lamellar spacing than the 22.16 at. pct. Zn alloy. The secondary inter-lamellar spacings are relatively closer to each other.

The effect of temperature on the inter-lamellar spacings are shown in the Δ T vs. 1/S and Δ T vs. ln S plots as shown in Figures 5 and 6 respectively.

The effect of temperature on the ratio of the secondary inter-lamellar spacings (S_2) to that of the primary (S_1) is also plotted along with the individual inter-lamellar spacings, in Figure 6.

The Δ T vs 1/S plot exhibits a linear relationship indicating that S increases with increase in the temperature. This is observed for both the alloys, during primary as well as secondary precipitation. The Δ T vs. ln S plots exhibit a

TABLE 2 : TEMPERATURE-INTER-LAMELLAR SPACING DATA FOR BOTH ALLOYS

Alloy	Temperature (°C)	Inter-lamellar spacing	
		Primary $S_1 \times 10^7$ m	Secondary $S_2 \times 10^7$ m
17.6 at.pct.Zn	487	7.24	13.19
	460	5.7	11.59
	436	4.925	10.72
	405	4.55	9.5
22.16 at.pct.Zn	520	8.027	16.4
	490	5.63	13.2
	460	4.82	11.834
	420	4.34	10.2
	400	3.86	9.3

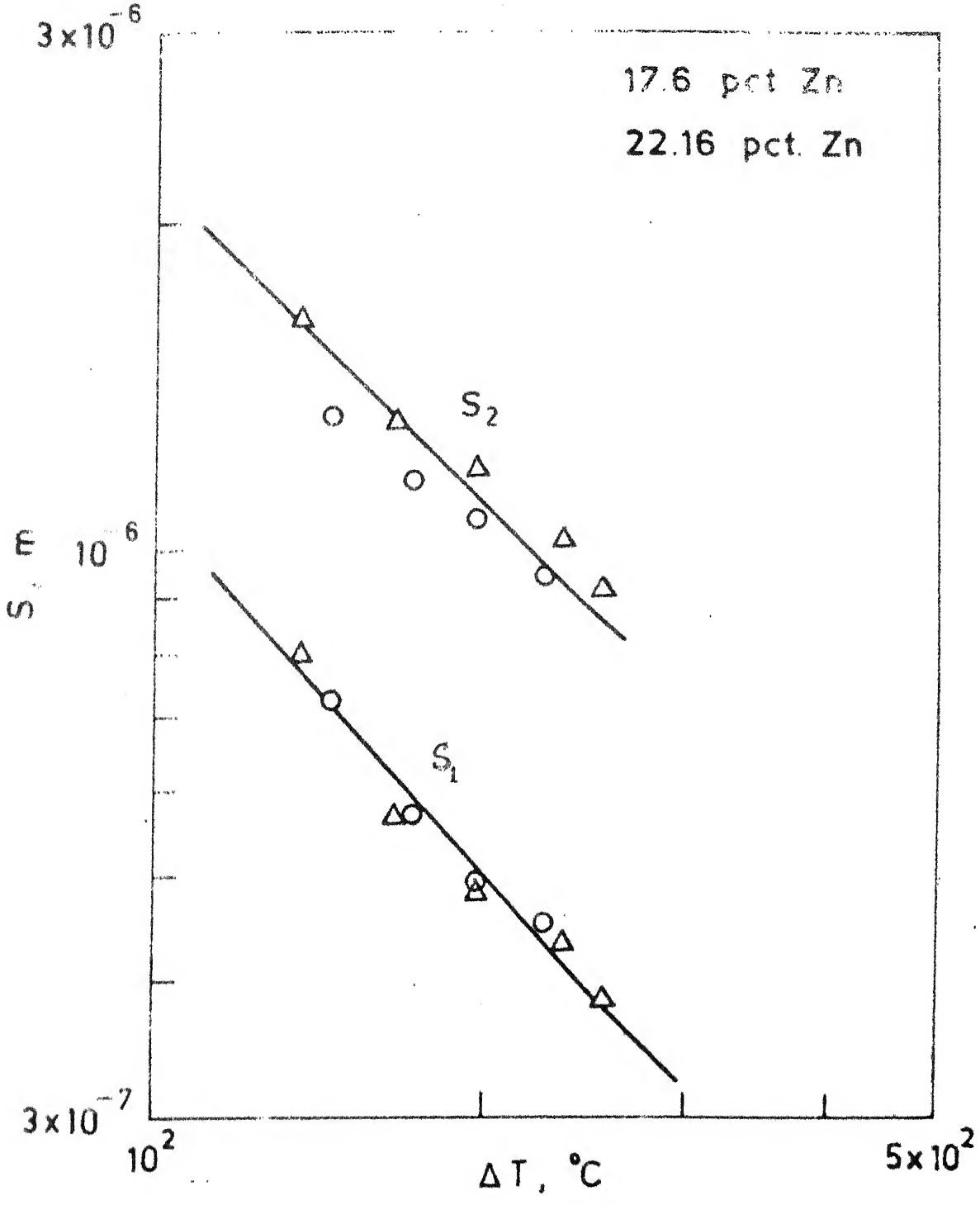

Fig. 7. Inter-lamellar spacing vs ΔT.

TABLE 3 : TEMPERATURE-DEGREE OF SEGREGATION DATA FOR BOTH ALLOYS

Alloy	Temperature (°C)	Degree of Segregation	
		Primary $P_{X_{Zn}}^{\alpha}$	Secondary $S_{X_{Zn}}^{\alpha}$
17.6 at.pct.Zn	487	0.1183	0.0925
	460	0.1049	0.08142
	436	0.0960	0.0725
	405	0.08892	0.065
22.16 at.pct.Zn	520	0.1340	0.1159
	490	0.1228	0.1072
	460	0.1157	0.1003
	420	0.1061	0.08947
	400	0.1010	0.085

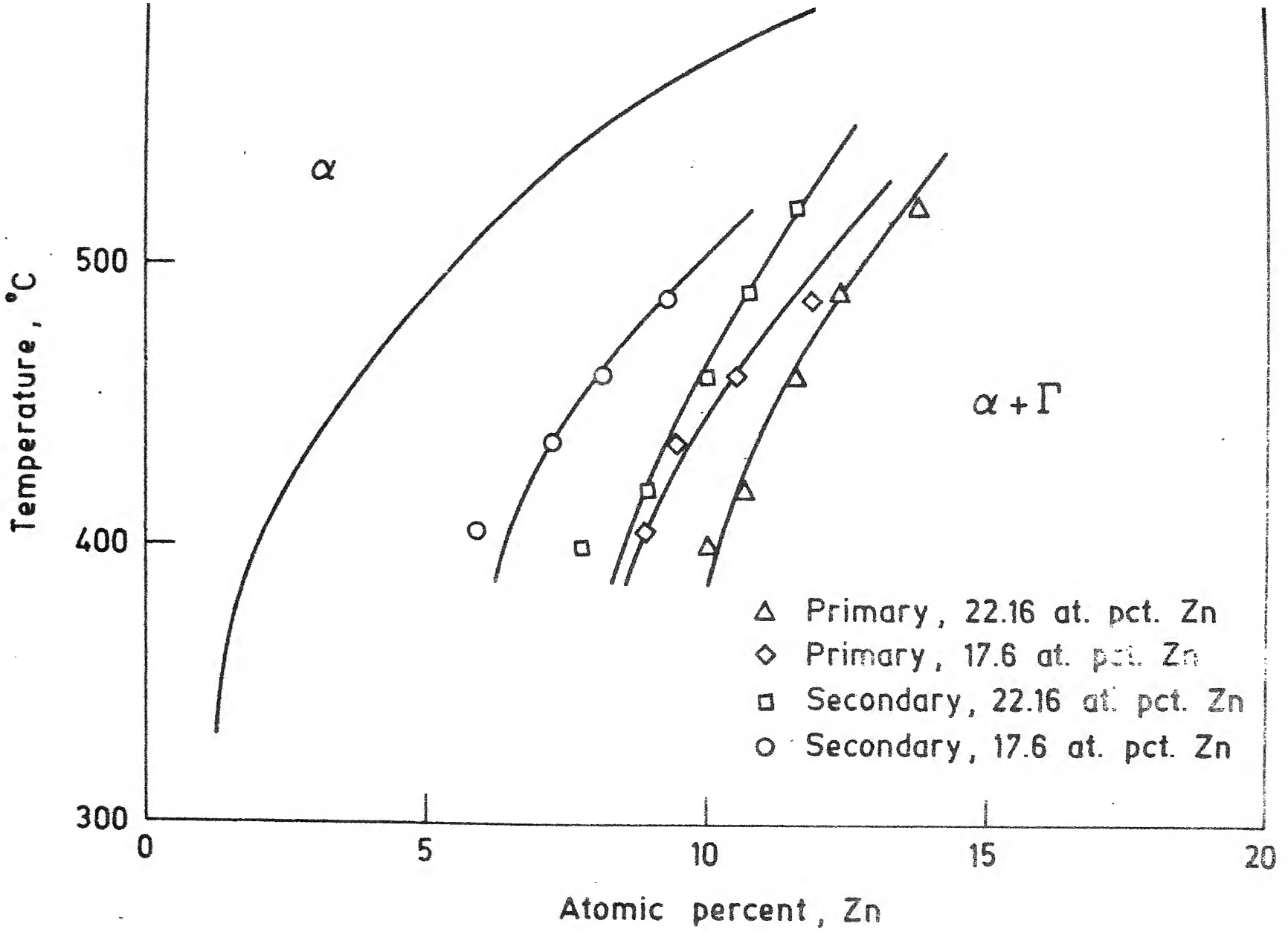

Fig. 8. Temperature vs degree of segregation.

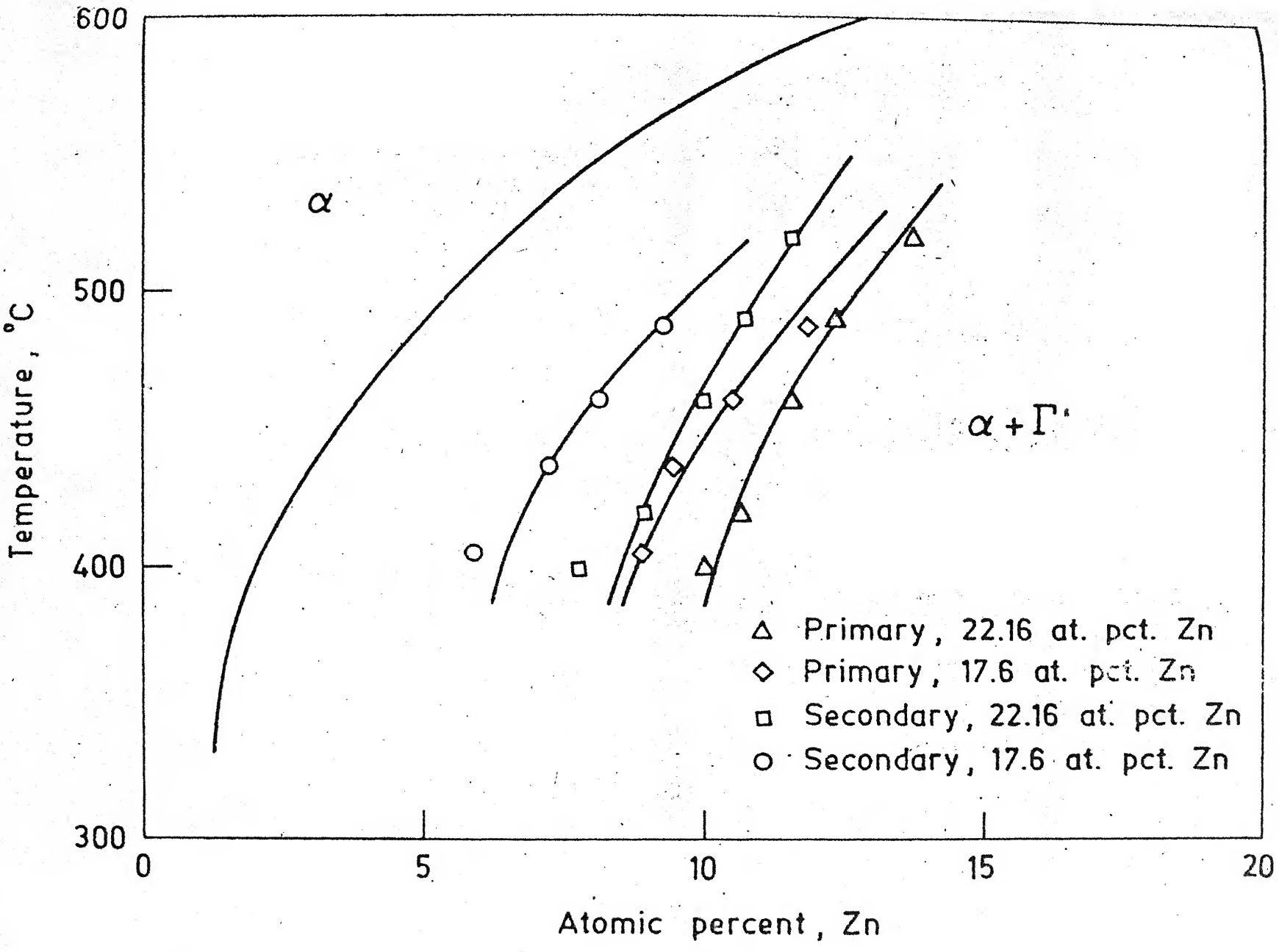

Fig. 8. Temperature vs degree of segregation

TABLE 4 : TEMPERATURE - $D^B_{Zn}\delta$ VALUES, CALCULATED USING DIFFERENT MODELS FOR BOTH PRIMARY AND SECONDARY PRECIPITATION, FOR BOTH ALLOYS

Alloy	Temp. (°C)	$D^B_{Zn}\delta$ x 10^{21} m^3/sec, (Primary)					$D^B_{Zn}\delta$ x 10^{21} m^3/sec, (Secondary)	
		Petermann-Hornbogen (eqn.28)	Turnbull (eqn.10)	Aaronson-1 (eqn.14)	Aaronson-2 (eqn.13)	Cahn (eqn.18)	Petermann Hornbogen (eqn.43)	Livingston -Cahn (eqn.36)
17.6 at.pct.Zn	487	61.8367	6.6593	1.4831	1.2792	0.3223	23.3115	21.1583
	460	17.3350	2.7258	0.6904	0.5912	0.2057	7.9415	10.77
	436	6.0795	1.1701	0.3251	0.2715	0.1086	3.2485	6.0032
	405	1.3204	0.2854	0.0857	0.0707	0.0317	0.6457	2.0640
22.16 at.pct.Zn	520	69.338	14.9529	3.6735	3.1050	1.3493	44.16	107.72
	490	33.481	8.3635	2.336	1.9364	0.9126	23.4668	61.87
	460	9.7308	2.604	0.8015	0.6562	0.3180	7.1722	29.8
	420	2.929	0.8825	0.3008	0.2423	0.1252	2.0738	7.1652
	400	0.9207	0.2953	0.1053	0.0841	0.0457	0.6557	0.3000

The diffusivity of Zinc, D^{B}_{Zn}, was estimated at 427°C, for all the models, from the ln $D^{B}_{Zn}\delta$ vs (Temperature)$^{-1}$ plots, as listed in Table 5, along with the activation energies. It is observed that Petermann-Hornbogen model has the highest rate of diffusion in the primary of both the alloys. The other models follow as Turnbull, Aaronson (1), Aaronson (2), and Cahn, as diffusivity decreases.

In the secondary, Livingston, Cahn model exhibits a higher rate of diffusion than Petermann-Hornbogen model. In both primary and secondary, the rate of diffusion is of the order of 10^{-12} m^2/sec.

The pre-exponential constant (D_o) was calculated for each model using the diffusion equation,

$$D = D_o \exp\left(-\frac{Q}{RT}\right) \qquad (45)$$

where,

$D = D^{B}_{Zn}$ = Diffusivity of Zinc,

Q = Activation energy,

R = 8.314 J/°K/mole,

T = 700°K.

The D_o values of individual models are also listed in Table 5. Each model exhibits D_o values of the same order, in both alloys, but different models have different orders of D_o values. Here, Petermann-Hornbogen model has the highest D_o values for both primary and secondary precipitates, in both the alloys.

TABLE 5 : ACTIVATION ENERGY (Q), DIFFUSIVITY (D^{B}_{Zn}), AND PRE-EXPONENTIAL CONSTANT (D_o) AT 700°K, FOR VARIOUS PRIMARY AND SECONDARY MODELS, FOR BOTH ALLOYS

Model	T°K	17.6 at. pct. Zn alloy			22.16 at. pct. Zn alloy		
		Q MJ/mole	$D_B \times 10^{-12}$ m^2/sec	D_o m^2/sec	Q MJ/mole	$D_B \times 10^{-12}$ m^2/sec	D_o m^2/sec
Primary							
Turnbull	700	0.15	1.45	0.2264	0.15	1.876	0.2929
Aaronson (1)	700	0.15	0.412	0.0643	0.14	0.604	0.0169
Aaronson (2)	700	0.15	0.346	0.054	0.14	0.506	0.0142
Cahn	700	0.14	0.1356	0.0038	0.14	0.253	0.0071
Petermann-Hornbogen	700	0.18	8.0	216.44	0.16	6.36	5.5365
Secondary							
Livingston-Cahn	700	0.13	8.28	0.0416	0.13	17.6	0.0884
Petermann-Hornbogen	700	017	3.98	19.32	0.16	4.58	3.987

The fraction P of the total free-energy used for precipitation is calculated from Cahn's equation (6),

$$P = \frac{3}{\sqrt{A}} \tanh\left(\frac{\sqrt{A}}{2}\right) - \frac{1}{2}\,\mathrm{Sech}^2\left(\frac{\sqrt{A}}{2}\right) \qquad (20)$$

where,

$$A = \frac{k\, v\, S^2}{D^B_{Zn}\, \delta}$$

The P values were determined both for primary and secondary precipitates, in both alloys, and are given in Table 6. As expected, the secondary precipitate is found to have larger P values than primary, at different aging temperatures. The difference between the two fractions (primary and secondary) are also given in Table 6. The 22.16 at.pct. Zn alloy is found to use a larger fraction of the total free-energy for primary precipitation than the 17.6 at.pct. Zn alloy. But, the 17.6 at.pct.Zn alloy uses a larger fraction for secondary precipitation than the 22.16 at.pct.Zn alloy, at lower temperatures (Δ T approximately 157°C). It is also observed that the fraction of total free energy used increases as the aging temperature decreases and the difference between the two fractions (primary and secondary) decreases as the aging temperature decreases, for both the alloys. The effect of aging temperature on the fraction of the total free-energy used for precipitation and the difference between the two fractions (primary and secondary), is shown in Figure 13.

TABLE 6 : TEMPERATURE - FRACTION OF THE TOTAL FREE ENERGY USED FOR PRECIPITATION DATA. FOR BOTH ALLOYS

Alloy	Temperature (°C)	P_1	P_2	P_2-P_1
17.6 at.pct.Zn	487	0.6547	0.8593	0.2046
	460	0.7280	0.8860	0.1579
	436	0.7559	0.8946	0.1387
	405	0.7763	0.9056	0.1293
22.16 at.pct.Zn	520	0.7759	0.8826	0.1066
	490	0.7883	0.8685	0.0802
	460	0.7920	0.8658	0.0732
	420	0.8010	0.8736	0.0736
	400	0.8094	0.8773	0.0679

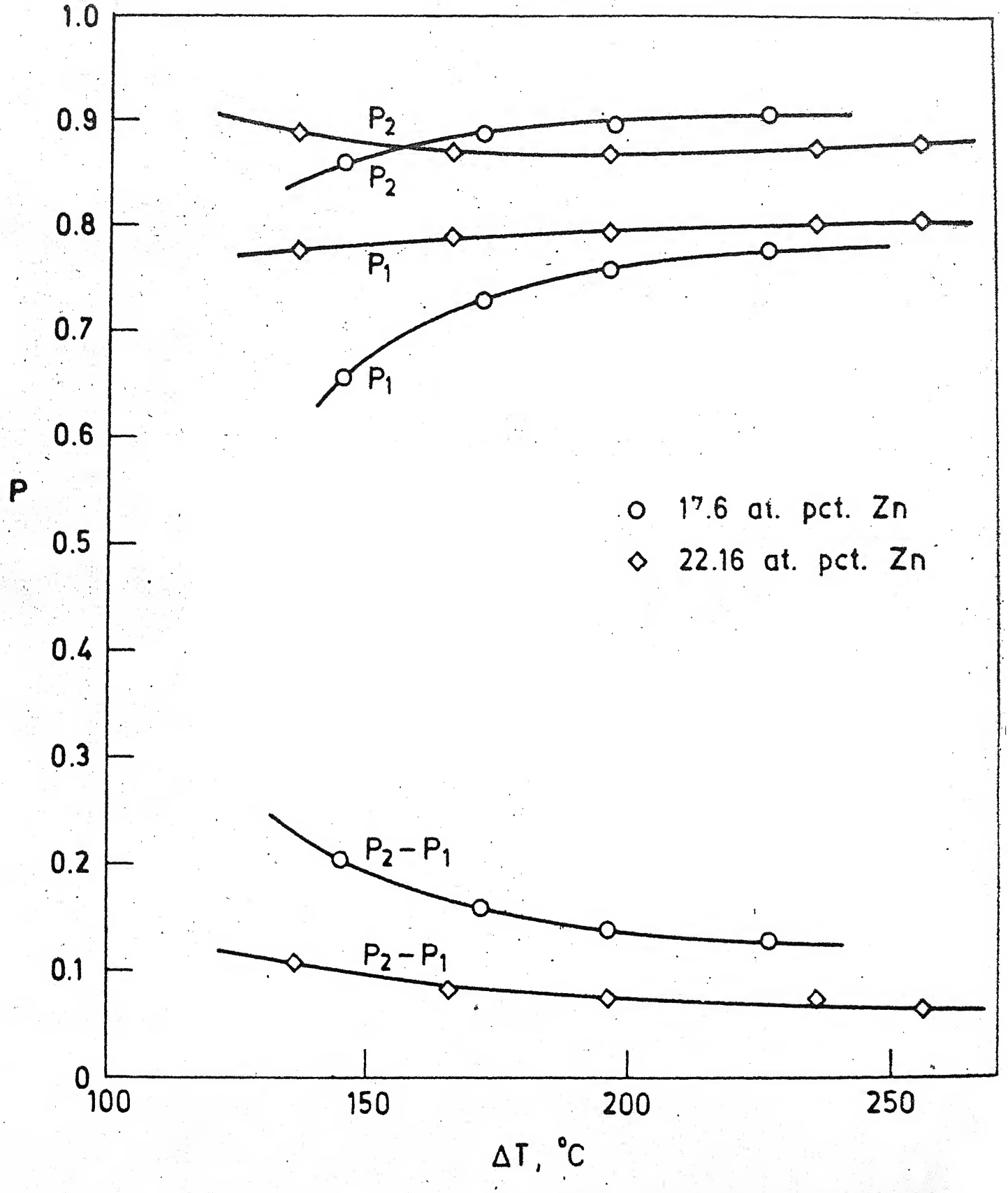
1.0
0.9
0.8
0.7
0.6
0.5
0.4
0.3
0.2
0.1
0
P
100
150
200
250
ΔT, °C
P2
P2
P1
P1
P2 − P1
P2 − P1
17.6 at. pct. Zn
22.16 at. pct. Zn

Fig. 13. P vs ΔT

Coarsening of discontinuous precipitates decreases the free-energy further, by decreasing the interfacial energy. The decrease in total free-energy of the coarsened or secondary precipitate has two components, 1. free energy change arising only from changes in composition of the phases, termed as the 'chemical free-energy change' and 2. the change in interfacial energy due to coarsening. The free energy changes, accompanying the primary and secondary reactions, ΔG_1 and ΔG_2 respectively, were calculated using the equation,

$$\Delta G_i = RT\left[{}^{1}X_B^{\alpha} \ln \frac{X_B^{\alpha}}{{}^{1}X_B^{\alpha}} + {}^{1}X_A^{\alpha} \ln \frac{X_A^{\alpha}}{{}^{1}X_A^{\alpha}}\right] \qquad \begin{matrix}\text{(first term of}\\ \text{equation 27)}\\ \text{(i=1,2)}\end{matrix}$$

according to Petermann-Hornbogen model (4).

ΔG_1 and ΔG_2 were obtained by substituting the corresponding X_B^{α} and X_A^{α} values for primary and secondary reactions. The difference between ΔG_2 and ΔG_1 gives a part of the chemical free energy used during secondary reaction alone (3). The values of $\Delta G_2 - \Delta G_1$ are listed in Table 7.

The amount of interfacial free energy released and used as a part of the chemical free energy required for the secondary reaction is given by $(\frac{2\gamma V_m}{S_2} - \frac{2\gamma V_m}{S_1})$, according to Fournelle (3). These values are also listed in Table 7.

It is observed that interfacial energies of both precipitates in both the alloys decrease with increase in aging temperature. They range from +13 to +27 J/mole for the primary and +6 to +11 J/mole for the secondary. This confirms

TABLE : 7 TEMPERATURE - INTERFACIAL ENERGY CHANGE - CHEMICAL FREE ENERGY CHANGE, FOR BOTH ALLOYS

Alloy	Temp. (°C)	ΔG_1 (J/mole)	ΔG_2 (J/mole)	$\frac{2\gamma V_m}{S_1}$ (J/mole)	$\frac{2\gamma V_m}{S_2}$ (J/mole)	$2\gamma V_m \left(\frac{1}{S_2} - \frac{1}{S_1}\right)$ (J/mole)	$\Delta G_2 - \Delta G_1$ (J/mole)
17.6 at.pct.Zn	487	-89.40	-213.13	13.63	7.81	-5.82	-123.73
	460	-139.42	-281.17	17.89	8.88	-9.01	-141.75
	436	-178.78	-315.02	20.90	9.60	-11.30	-136.24
	405	-205.64	-401.23	23.33	10.82	-12.51	-195.59
22.16 at.pct.Zn	520	-187.64	-293.49	12.99	5.93	- 7.06	-105.85
	490	-233.88	-343.82	18.40	7.88	-10.52	-109.94
	460	-272.55	-389.51	21.56	8.81	12.75	-116.96
	420	-319.84	-454.83	23.94	10.19	-13.75	-134.99
	400	-352.51	-492.39	26.86	11.17	-15.69	-139.88

that the interfacial energy decreases with discontinuous coarsening.

The change in total free energy also decreases with increase in aging temperature, for both precipitates, in both alloys. The change in total free energy ranges from -89 to -352 J/mole for the primary and from -213 to -492 J/mole for the secondary. This confirms that the total free energy also decreases with discontinuous coarsening.

The chemical free energy change due to discontinuous coarsening also decreases with increase in aging temperature, in both alloys. It ranges from -105 to -195 J/mole. On comparison with the interfacial energy changes, it is observed that the chemical free energy change contributes to a much larger extent for the driving force of discontinuous coarsening, than that from the change in interfacial energy. The values of the changes in chemical free energy and interfacial energy show the chemical free energy available for the discontinuous coarsening reaction to be approximately two orders of magnitude greater than the corresponding interfacial energy terms.

CHAPTER 4

DISCUSSION

Coarsening in Fe + Zn alloys, used for this investigation, has been found to occur by discontinuous mode. Similar to other alloy systems the growth distance during coarsening increased with the time of aging. The initial precipitation is also observed to be of the discontinuous mode.

The coarsened cells with large interlamellar spacings were surrounded by primary cells with relatively finer lamellae. These coarsened cells of the secondary precipitates exhibited much slower growth rates compared to the primary in both alloy compositions.

Since the effective diffusion distance is taken to be equal to half the inter-lamellar spacing (6), and the inter-lamellar spacings are higher for the secondary as compared to the primary, the Zn atoms have to diffuse through a larger distance in the case of secondary precipitation. Moreover, the precipitates phase associated with the primary has to dissolved ahead of the secondary cell front. This explains to some extent the slower rate of growth observed for the secondary precipitate.

Both primary and secondary precipitations involve the diffusion of Zn in the boundary. The growth rates are observed to increase for both primary and secondary, as the aging temperature increases upto 490°C in both alloys.

This can be attributed to the fact that diffusivity of Zn increases with increasing aging temperature, according to the diffusion equation,

$$D = D_o \exp -(-\frac{Q}{RT}) \qquad (45)$$

Beyond 490°C, the growth rate is again observed to decrease with increasing temperature. In this region, supercooling (Δ T) becomes predominent and since it decreases as aging temperature increases, the growth rate again starts decreasing.

The primary and secondary growth velocities are observed to increase with increasing original alloy composition. Both velocities are greater for the 22.16 at. pct. Zn alloy when compared to the 17.6 at.pct.Zn alloy. This can be explained on the basis of increased grain boundary concentration gradient with increase in Zinc content of Iron. As the supersaturation increases, the net flow of solute atoms in the advancing cell front increases and so the precipitation rate is relatively higher when compared to an alloy with a lesser super-saturation.

Scatter in the data points for the distance travelled by the moving cell boundary can be seen from Figures 2 and 3. This is expected in polycrystalline specimens and can be explained as follows: the motion of a cell boundary is related to the misorientation of the two grains, across the grain boundary. The grain boundary mobility increases with the misorientation. When comparison is made between twist

boundaries, the migration velocity increases with increasing misorientation, to a certain limit. Since discontinuous phase transformation is controlled by migration of grain boundaries, different cell boundaries will cover different distances, depending on the extent of misorientation between the grains, across different grain boundaries. These distances differ substantially from one region to the other. Since the data represented here is an average of readings taken randomly, some scatter in the data is expected.

The primary growth velocities obtained in this investigation were compared to those obtained by Speich (9). Speich had investigated the 15.2 at.pct.Zn and 23.5 at.pct.Zn alloys. The 17.6 at.pct.zn. alloy of this investigation was compared to the 15.2 at.pct.Zn alloy and the 22.16 at.pct.Zn alloy was compared to the 23.5 at.pct.Zn alloy of Speich (9). The 17.6 at.pct.Zn alloy showed relatively higher primary growth velocities than the 15.2 at.pct.Zn alloy, as expected. The 22.16 at.pct.Zn alloy showed lower growth velocities than the 23.5 at.pct.Zn alloy. In all the alloys, the primary velocities were of the same order (10^{-9}m/sec). The growth velocities were compared at their relative aging temperatures.

The inter-lamellar spacings are found to increase with increase in the aging temperature at constant Zn content, and with decrease in Zn content of the original alloy at constant temperature, both during primary and secondary cell growth./. With increase in aging temperature, the diffusivity

at constant temperature

is increased and so the solute atoms are able to diffuse through longer distances, thus resulting into higher interlamellar spacings. With decrease in Zn content of the original alloy, the growth velocity is observed to decrease with decrease in the Zn content of the alloy allowing time for solute to move longer distances at a given temperature. This results in an increase of the interlamellar spacing.

The primary interlamellar spacings of both alloys were compared to those reported by Speich (9), for 15.2 at. pct.Zn and 23.5 at.pct.Zn alloys. The 17.6 at.pct.Zn alloy exhibited lower interlamellar spacings compared to the 15.2 at. pct.Zn alloy, and the 22.16 at.pct.Zn alloy exhibited larger interlamellar spacing compared to the 23.5 at.pct.Zn alloy, at corresponding aging temperatures, confirming that the interlamellar spacing data experimentally observed in the present study are quite consistent with the results published by Speich (9). The primary interlamellar spacings when compared to those reported by Predal, et.al. (24), for the 10 at.pct.Zn alloy, exhibit lower interlamellar spacings as expected.

The degree of segregation behaviour, as observed in the present investigation, is supported by the observations made by Speich (9), on the primary precipitation behaviour. The values of the degree of segregation for the primary reaction could be compared to the corresponding alloys. The 17.6 at.pct. Zn alloy shows a higher degree of segregation than the

15.2 at.pct.Zn alloy, and the 22.16 at.pct.Zn alloy shows a lesser degree of segregation than the 23.5 at.pct.Zn alloy. The degree of segregation decreases as the isothermal transformation temperature increases.

The degree of segregation increases as Zn content in the original alloy increases. An increase in Zn content has been observed to accelerate the rate of the transformation and therefore lesser time will be available to disperse the solute for the alloy with higher Zn content. This implies that the degree of segregation will increase with increasing Zn content of the original alloy.

The secondary precipitates, exhibiting a larger volume fraction of the γ-phase then the primary, in both alloys, can be explained on the basis of the Thomson-Freundlich equation, which is a modification of the Gibbs-Thomson equation,

$$X_B^{\alpha} = X_B^{\alpha} \left(1 + \frac{2\gamma V_m}{SRT}\right) \qquad (47)$$

This equation implies that with increase in the interlamellar spacing, the degree of segregation would decrease, at a constant temperature. This accounts for the fact that secondary has a lesser degree of segregation than the primary. Combining equations (47) and (44), we see that, f (volume fraction of γ phase) increases with increasing interlamellar spacing.

In order to evaluate the kinetics of cellular transformation in these alloys, D_B was plotted against the reciprocal of absolute temperature, Figures 9, and 10.

The Petermann-Hornbogen model is expected to give a higher $D_B \delta$ value since it is increased by a factor of $\frac{RT}{\Delta G}$. This additional factor is contributed by the assumption that the driving force for the precipitation reaction is the chemical free-energy available. Turnbull (6), Aaronson 1(7), Aaronson 2(7) and Cahn's (8) models have comparable $D_B \delta$ values, decreasing in the given order by a small factor, contributed by the degree of segregation.

Figures 11 and 12 represent the $D_B \delta$ vs $\frac{1}{T}$ plots for the secondary reaction in the 17.6 at.pct.Zn and 22.16 at.pct. Zn alloy, respectively. Here also, the increase in $D_B \delta$ with aging temperature is observed, which due to the increase in diffusivity with temperature. The Livingston and Cahn model is observed to show higher $D_B \delta$ values at all temperatures in the 22.16 at.pct.Zn alloy but the same is observed only below 490°C approximately in the 17.6 at.pct.Zn alloy. The $D_B \delta$ values of Livingston and Cahn model are higher since they involve a factor of S_2^2 (S_2 = interlamellar spacing of the secondary) which results from the consideration that only the decrease in interfacial energy, contributes to the driving force for the secondary reaction. The $D_B \delta$ values of the Petermann-Hornbogen model are reduced below that of Livingston and Cahn model since the factor $D_B \delta$ is dominated by $v_1 S_1^2$ instead of $v_2 S^2$ primary growth velocity v_1 being two orders of magnitude higher than v_2 giving rise to $v_1 S_1^2 >> v_2 S_2^2$.

The $D_B \delta$ values increasing beyond those of Livingston and Cahn, above 490°C, in the 17.6 at.pct.Zn alloy, may be due to an error in the estimation of S_1 and S_2 at 487°C. The $D_B \delta$ value corresponding to the aging temperature 487°C is abnormally high in the Petermann-Hornbogen model.

The activation energies (Q) for the cell boundary migration according to different models of both primary and secondary, have been determined from the temperature dependence of the diffusivity. The Q values range from 0.14 to 0.18 MJ/mole for the primary. Results reported by Howarth, Wriedt and Gula (27), indicate that the AE for volume diffusion of Zn in Fe is approximately 0.265 MJ/mole. The observed values of the present investigation fall in the range of half to two-third of the volume diffusion value. This indicates that the primary and secondary cellular reactions are controlled by the diffusion of Zn through the grain boundary. Speich (9) has obtained a value of 0.135 MJ/mole using the Cahn model for the primary reaction in Fe-Zn alloys. In the present investigation, both the alloys exhibited an activation energy of 0.14 MJ/mole, in the Cahn model of primary reaction. The two values are comparable. This affirms that Zn diffuses through the boundary and not through the lattice for the primary reaction.

The activation energy of the primary reaction in both alloys, obtained here for the Aaronson (1) model, was compared to that obtained by Predel (24) for the 10 at.pct.Zn alloy.

Predel reports a value of 0.15 MJ/mole, which are in good agreement with the results of the present investigation.

The Q values of the secondary are also comparable to that of the primary, which range from 0.13 to 0.17 MJ/mole. This indicates that the secondary reaction also is controlled by boundary diffusion of Zn and not lattice diffusion.

Since the driving force has been found to decrease rapidly with the increase in aging temperature, the $D_B \delta$ value at higher aging temperatures is quite high in the Petermann-Hornbogen model (4). This results into a higher Q value, although the data fits better in the whole range of temperature.

The D_B (boundary diffusivity of Zn) value was calculated for all the models, in both primary and secondary of both alloys, at 700°K (427°C). 'δ' (the boundary layer thickness) being taken as constant $=5 \times 10^{-10}$m, after Speich (9), the estimated D_B values showed the same behaviour as that of the $D_B \delta$ values.

Since the Q, D_B, T and R values are known, the D_o value was estimated for all the different models investigated in both the alloys. Since $D_o = D_B \exp \frac{Q}{RT}$, the Petermann-Hornbogen model of primary and secondary of the 17.6 at.pct. Zn alloy showed abnormally high D_o values. One of the possible causes of the abnormally high D_o values could be the estimate of ΔG value from the mole fraction data.

The fractions of the total available chemical free-energy, used for both primary and secondary reactions, P_1 and P_2 respectively, were calculated for both the alloys using equation (20). The P_1 values range from 0.6547 to 0.7763 for the 17.6 at.pct.Zn alloy and from 0.7759 to 0.8094 for the 22.16 at.pct.Zn alloy, which are comparable to the values obtained by Speich (9). The P_2 values were higher than P_1 as expected, since more amount of the available energy would be used up for any further transformation, beyond the primary reaction. They ranged from 0.8593 to 0.9056 for the 17.6 at.pct.Zn alloy, and from 0.8826 to 0.8773 for the 22.16 at.pct.Zn alloy.

The fraction of the driving force during primary reaction, P_1, increases with decrease in the aging temperature. It appears that a larger proportion of the total available chemical free energy is used in the reaction. It should be mentioned that as the temperature decreases, the total available, ΔG_o, increases. It is further to be indicates that as the temperature decreases, the proportion of the available chemical free energy used to form $\alpha - \Gamma$ interface increases.

This secondary reaction involves two processes: (i) dissolution of the primary ahead of the reaction front and (ii) redistribution of the solute atoms at the reaction front. During secondary coarsening, a part of the driving force from the free energy release at the primary secondary reaction front. Since the 22.16% alloy has lower primary interlamellar

spacing than the 17.6% alloy, and the secondary interlamellar spacings are the same in two alloys under consideration, there is a larger amount of interfacial free energy released per mole in the 22.16% alloy. This should give a higher driving force for the secondary reaction in the 22.16% alloy.

The difference of chemical free-energy and the interfacial free energy between the primary and secondary reactions were calculated for both the alloys from their respective equations. A comparison between the two values, $\Delta\gamma$ (interfacial free energy change) and ΔG, (chemical free-energy change), shows that the chemical free energy change for the secondary reaction is nearly two orders of magnitude greater than that of the corresponding interfacial energy changes. These results are in good agreement with those of RA Fournelle (3) who has reported results for the Fe-Ni-Ti alloy. This implies that change in the chemical free energy has major contribution towards the driving force for the secondary reaction. This result further improves the validity of the Petermann-Hornbogen model for the secondary precipitation.

The morphology of both primary and secondary precipitations are shown from Figures 14-17. Figures 14 and 15 show the growth sequence of the primary and secondary precipitates of the 17.6 at.pct.Zn alloy, aged at 487°C, respectively, for different lengths of time. It is observed that in either mode, the volume fraction of the precipitate increases with increase in aging time. The nucleation of the primary precipitates are observed at the grain boundaries, as the grain boundaries act as

Figure 14 : Primary Growth Sequence

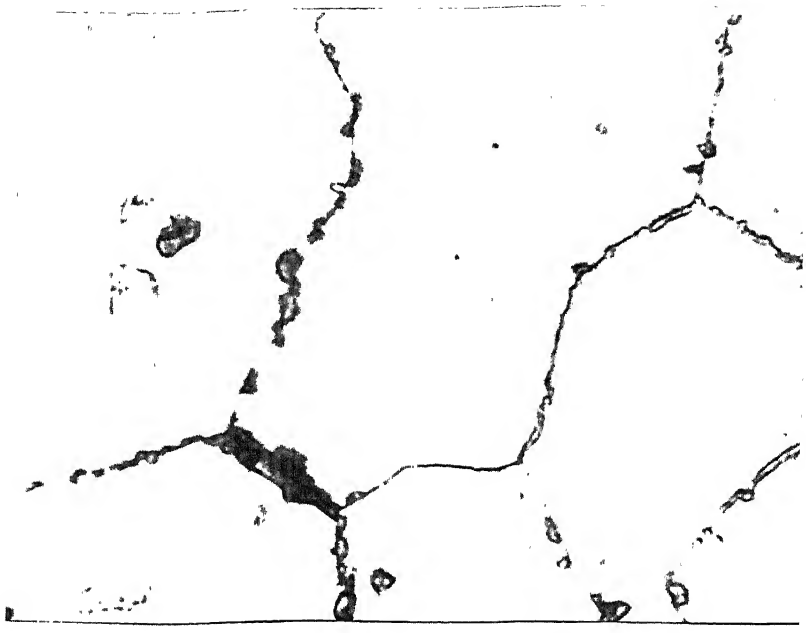

Fig.14A : 17.6 at.pct.Zn sample treated at 487°C for 10 minutes (M = X)

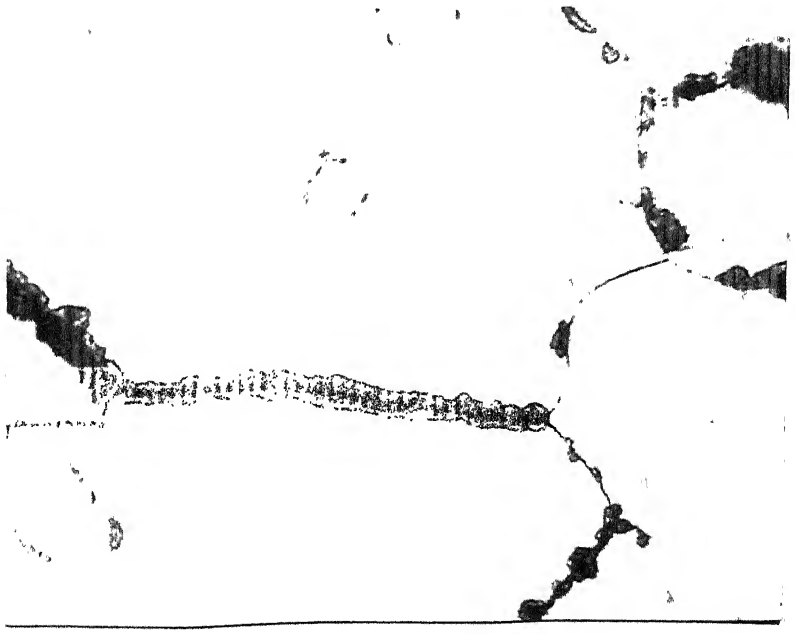

Fig.14B : 17.6 at.pct.Zn sample treated at 487°C for 20 minutes (M = /60 X)

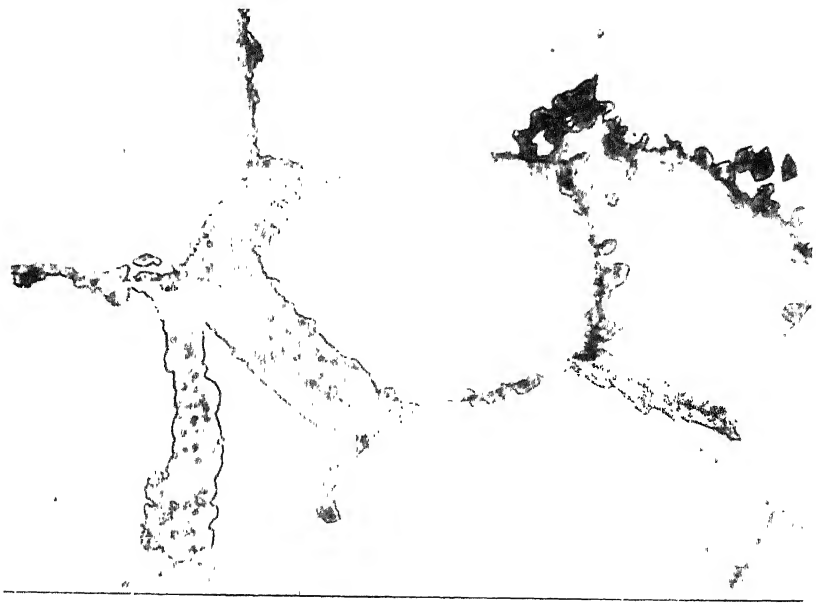

Fig.14C : 17.6 at.pct.Zn sample treated at 487°C for 40 minutes (M = X)

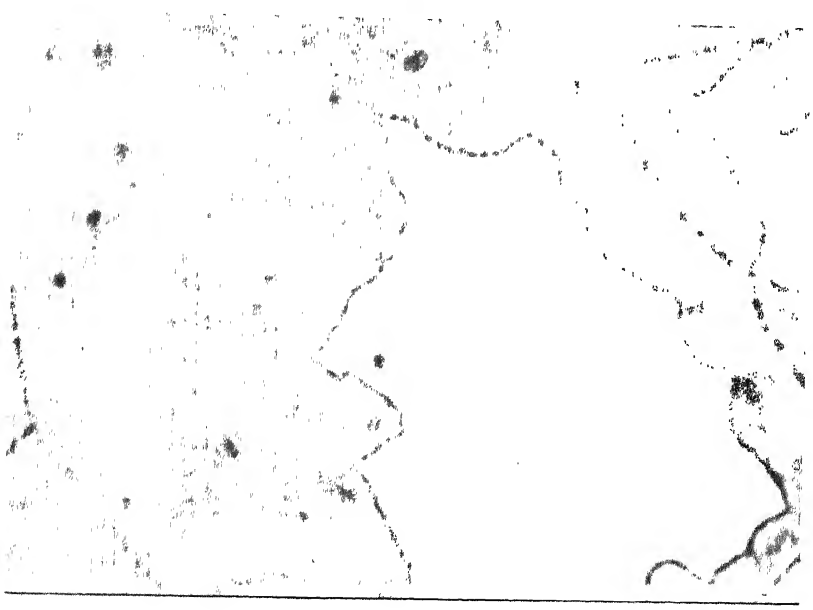

Fig.14D : 17.6 at.pct.Zn sample treated at 487°C for 240 minutes (M = X)

Figure 15 : Secondary Growth Sequence

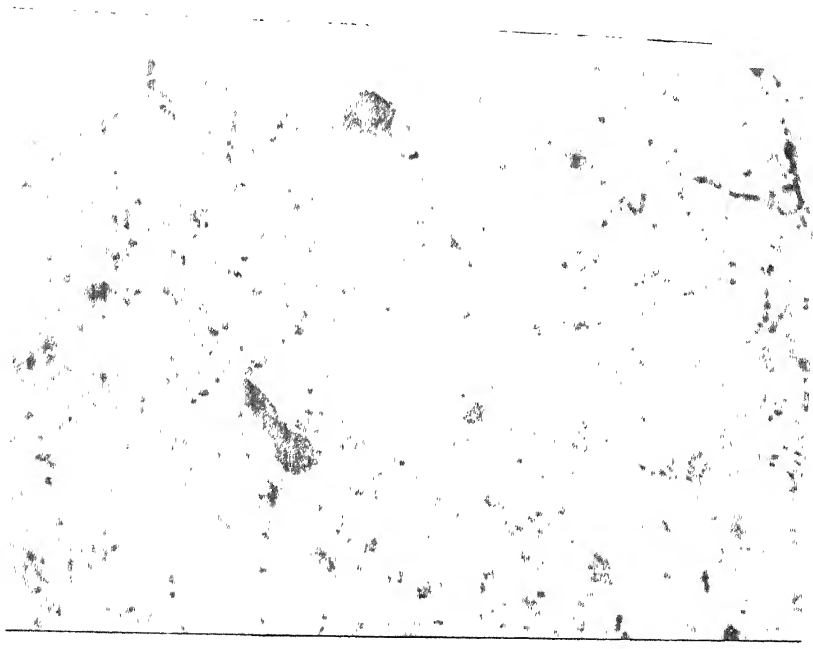

Fig.15A : 17.6 at.pct.Zn sample treated at 487°C for 40 hours (M = [illegible] X)

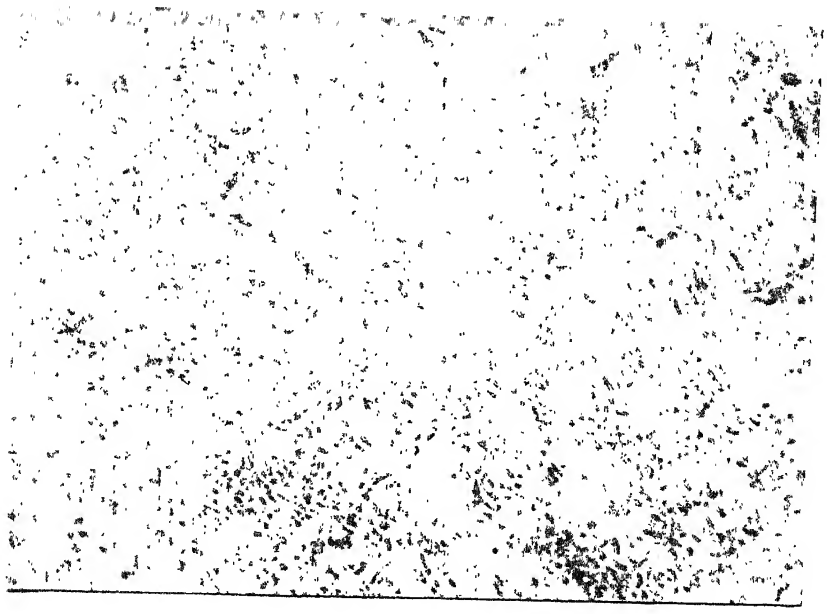

Fig.15B : 17.6 at.pct.Zn sample treated at 487°C for 73 hours (M = 650 X)

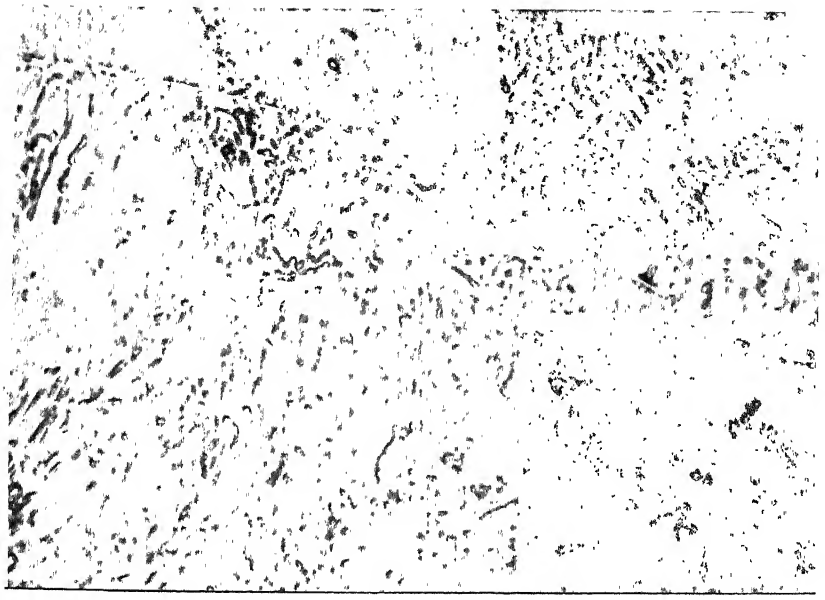

Fig.15C : 17.6 at pct.Zn sample treated at 487°C for 117 hours (M = X)

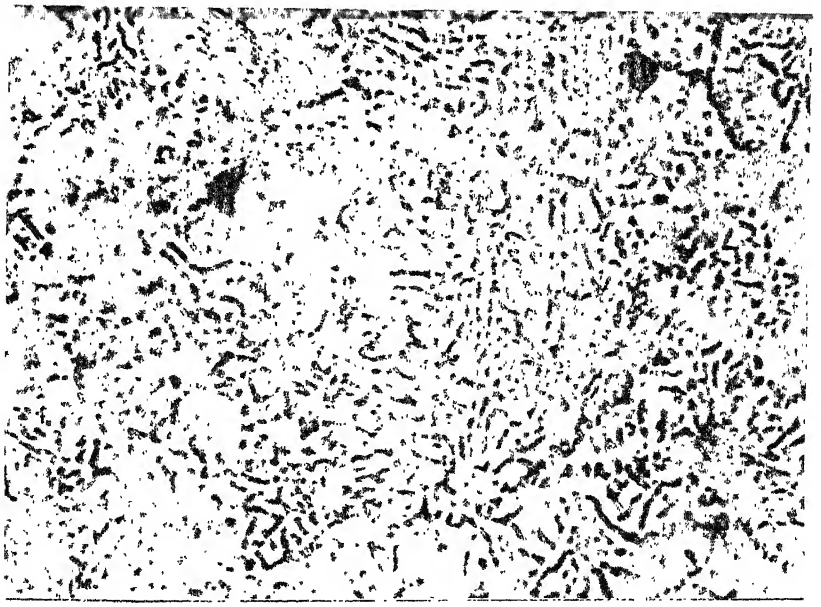

Fig.15D : 17.6 at.pct.Zn sample treated at 487°C for 216 hours (M = X)

heterogeneous nucleation sites, reducing the energy required for nucleation.

Figures 16 and 17 show the mechanisms of growth of the primary and secondary precipitations respectively. It is observed that the primary precipitation starts with the nucleation at the grain boundary. This is indicated by the tiny serrations appearing on the grain boundary (Figure 16A). The boundary migration is then initiated with certain regions of the boundary migrating forward (Figures 16B and C), dragging the nearby areas along with them. As the boundary migrates, it leaves behind the transformed region containing alternate lamellae of depleted- α and the Zn rich η phases (Figures 16D). The grain boundaries with large misorientation are found to migrate faster than the grain boundaries with smaller misorientation (Figure 16E). The migration of the boundary ceases in the regions where it impinges with another advancing boundary. The photographs obtained in Figure 16 are from a 22.16 at.pct.Zn alloy sample, aged at 420°C for 60 minutes. These observations are in good agreement with those made by Tu (12).

The nucleation of secondary precipitate shown in Figure 17, indicate three possible sites:

i) at the original α-Fe grain boundaries (Figs.17A,B,C,D)

ii) at the impinged region of two advancing fronts (Figs.17E,F,G)

iii) at the impinged region of an advancing front and an original grain boundary, (Figs.17H, I).

Figure 16 : Primary Mechanism

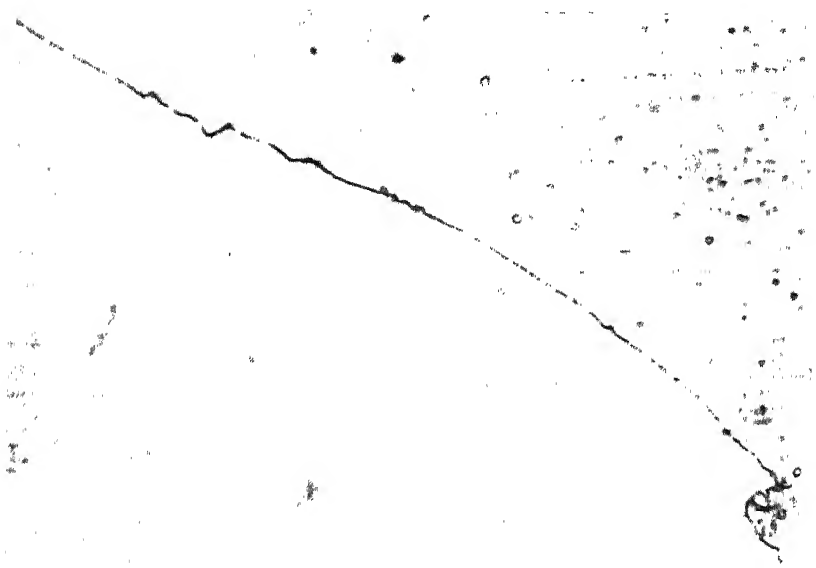

Fig.16A : 22.16 at.pct.Zn sample treated at 420°C for 60 minutes (M = X)

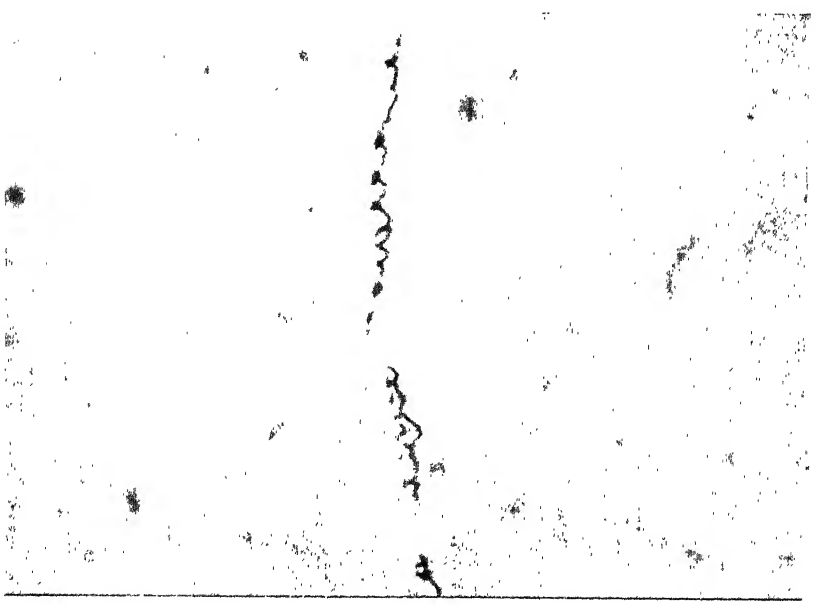

Fig.16B : 22.16 at.pct.Zn sample treated at 420°C for 60 minutes (M = X)

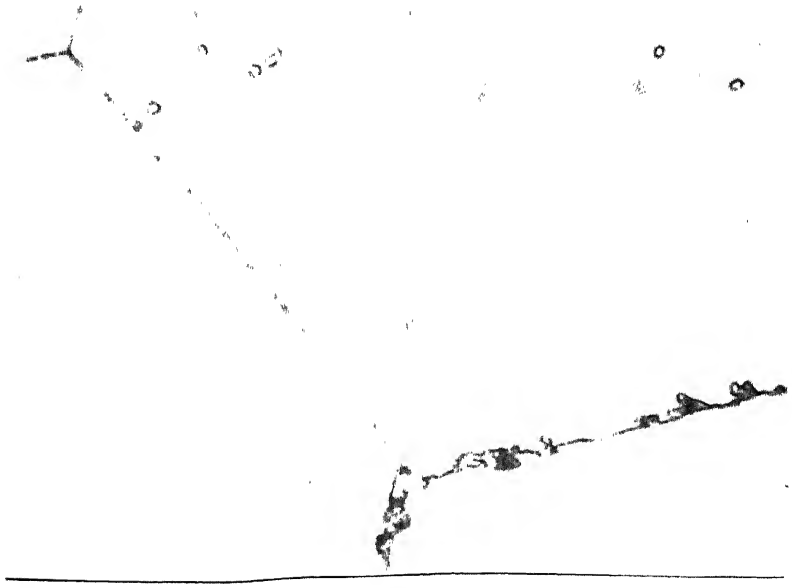

Fig.16C : 22.16 at.pct.Zn sample treated at 420°C for 60 minutes (M = X)

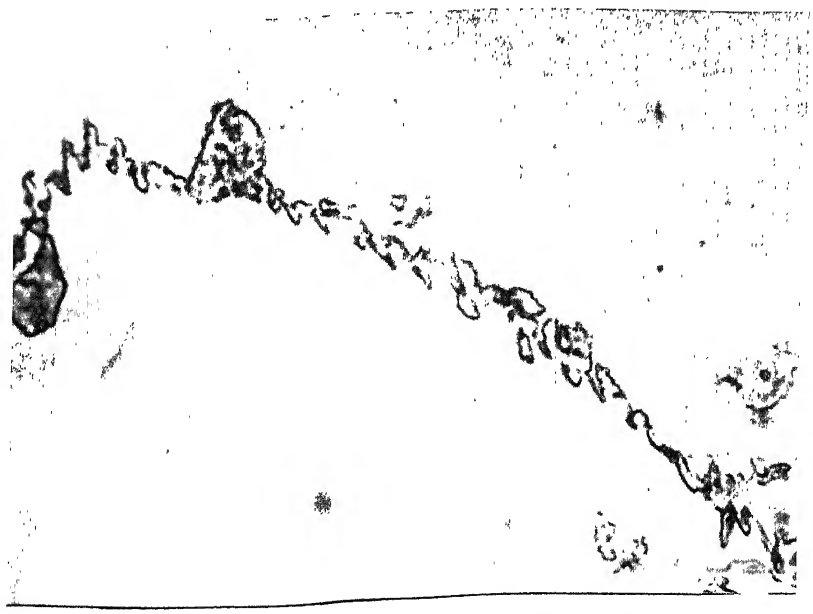

Fig.16D : 22.16 at.pct.Zn sample treated at 420°C for 60 minutes (M = X)

Fig.16E : 22.16 at.pct.Zn sample treated at 420°C for 60 minutes (M = [illegible] X)

Figure 17 : Secondary Mechanism

Fig.17A: 17.6 at.pct.Zn sample treated at 487°C for 73 hours (M = X)

Fig.17B : 17.6 at.pct.Zn sample treated at 487°C for 73 hours (M = X)

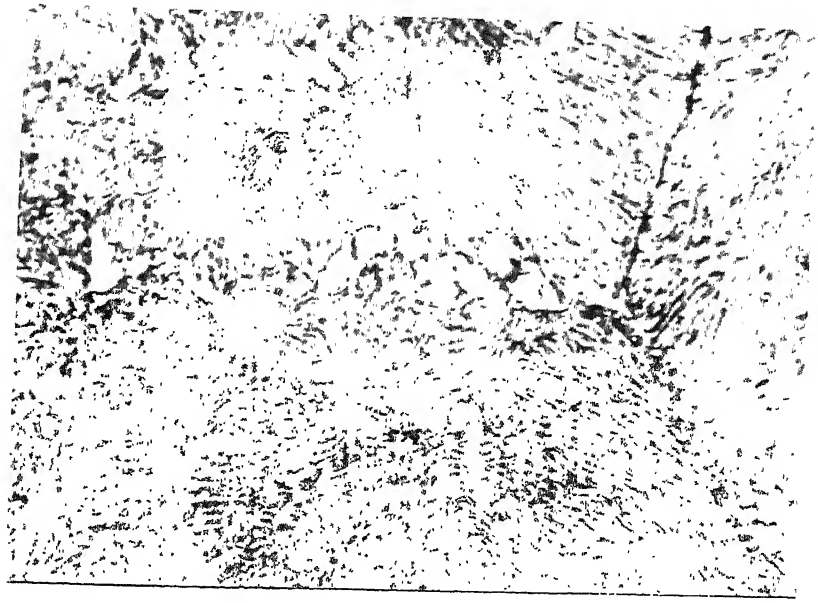

Fig.17C : 17.6 at.pct.Zn sample treated at 487°C for 73 hours (M =)

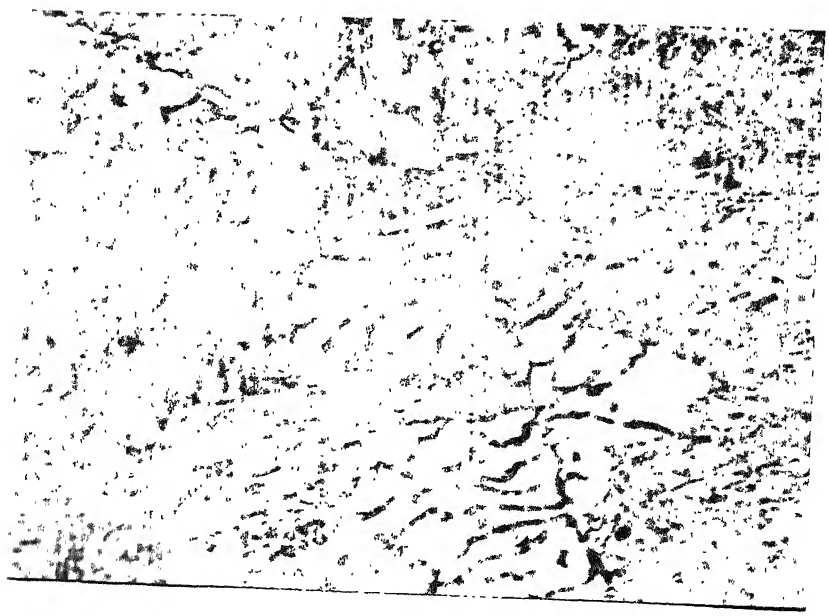

Fig.17D : 17.6 at.pct.Zn sample treated at 487°C for 73 hours (M = X)

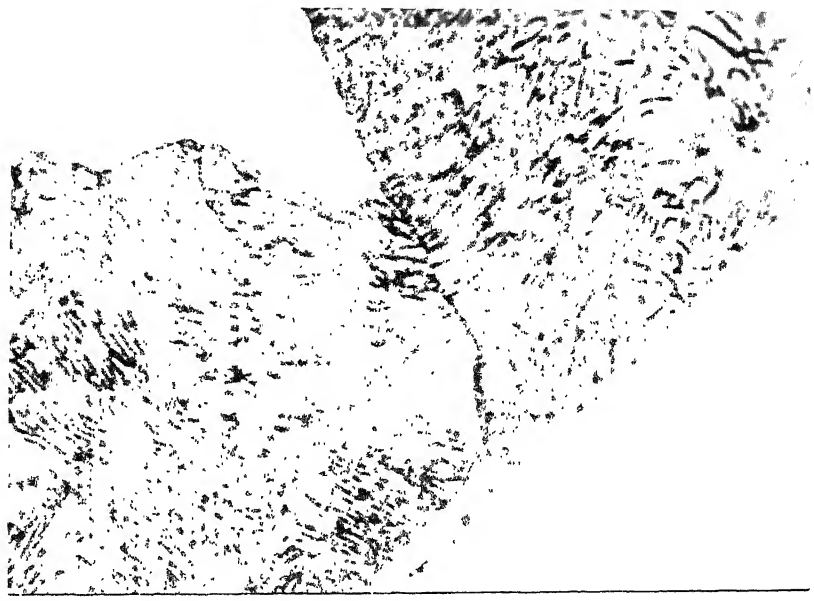

Fig.17E : 22.16 at.pct.Zn sample treated at 520°C for 60 minutes (M= X)

Fig.17F : 22.16 at.pct.Zn sample treated at 520°C for 60 minutes (M = X)

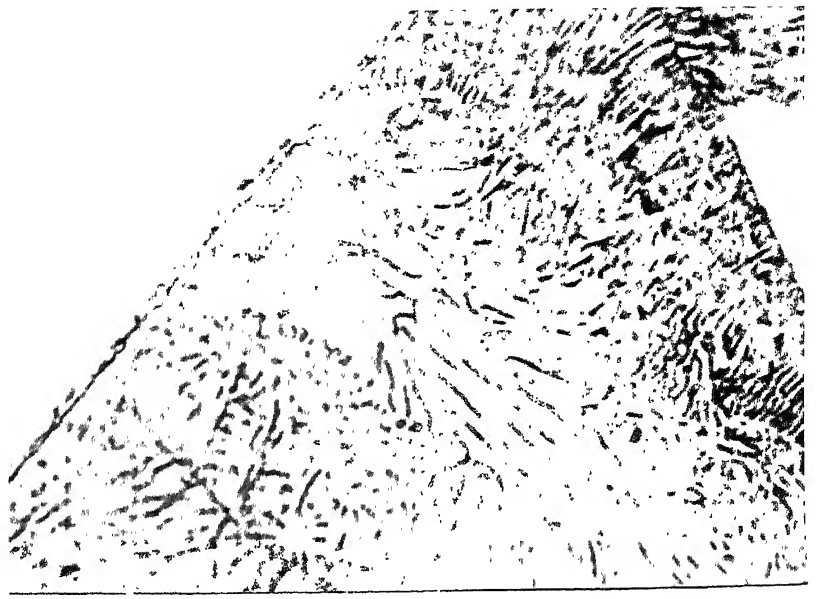

Fig.17G : 22.16 at.pct.Zn sample
treated at 520°C for
60 minutes (M= X)

Fig.17H : 17.6 at.pct.Zn sample
treated at 487°C for
73 hours
(M = X)

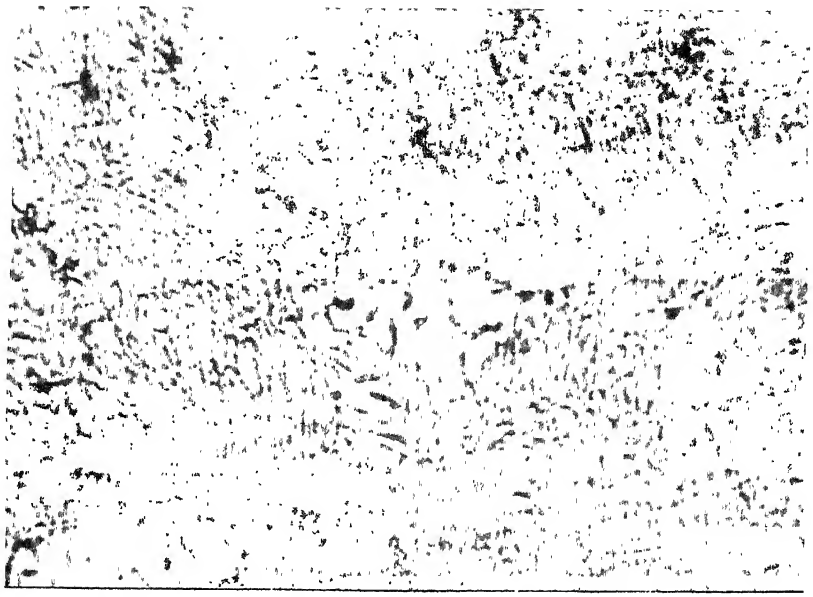

Fig.17I : 17.6 at.pct.Zn sample
treated at 487°C for
73 hours (M = X)

A large number of areas, where the secondary precipitate had nucleated at the triple junctions of grain boundaries were observed, (Figure 17A). This can be attributed to the fact that nucleation at the edges of grain boundary (where the three boundaries meet) requires much smaller energy compared to that required for homogeneous nucleation or on the boundary surface.

The secondary cells are observed to nucleate even before the primary reaction is complete. This is shown in Figures 17E,F,G.

Two mechanisms for the initiation of secondary cells at the original α-Fe grain boundaries are shown in Figures 17A,B and 17C,D. In the mechanisms depicted in Figures 17A,B, a cell originating at one α-Fe grain boundary grows into the origin of a cell, originated at another α-Fe boundary, and begins to decompose the cell according to the second reaction. Figures 17C,D represent an extension of an 'S' mechanism which has been observed in many systems exhibiting discontinuous precipitation (21 and 25). In this mechanism, adjacent segments of a boundary between two supersaturated grains are observed to migrate, into opposite grains leaving behind lamellae, oriented with respect to the grains from which they grew (Fig.17C). Continuing this growth, they pivot about a common point on the original α-Fe grain boundary in such a way that the advancing boundary of each cell eventually grows into the origin of its counterpart at the original α-Fe grain boundary (Fig.17D), and begins decomposing it by the secondary

reaction. Both of these mechanisms not only account for the appearance of secondary cells prior α-Fe grain boundaries but also guarantee that the advancing boundary of the second cells will have the same characteristics as the first cell from which it formed. These photographs, 17A to D, were obtained from a 17.6 at.pct.Zn alloy, aged at 487°C, for 73 hr.

Growth of secondary cells at the primary cell intersection (Figure 17E,F,G) requires the creation of a mobile boundary when the two primary cells intersect. This is achieved by the change in growth velocities at the intersected region due to the overlapping of two solute concentration fields, when the two primary cells intersect. This was observed in a 22.16 at. pct.Zn alloy sample, aged at 520°C for 60 minutes, whose photographs are shown.

The formation of secondary lamellae at the impinged region of a primary front and an original grain boundary is found in very few regions. This may be due to the fact that very few original grain boundaries remain without nucleating and advancing, before another mobile grain boundary can impinge upon it. The possibility could be expected in very small grains, whose boundaries are low angled in certain regions and sufficiently high angled in other regions for high mobility, since the boundary mobility increases with the angle of misorientation. An example of such a region, observed in a 17.6 at.pct.Zn alloy specimen, aged at 487°C for 73 hours, is shown in Figure 17H and I.

The mechanisms for secondary precipitation from the original α-Fe grain boundary and from the impinged region of two advancing fronts are in good agreement with those of Fournelle (21), and Williams, et.al. (25).

The secondary precipitate exhibiting larger inter-lamellar spacings can be observed in Figure 18A. The dark, almost parallel secondary lamellae with larger spacings are surrounded by a faint region consisting of closely - spaced primary lamellae. This photograph was taken from a 17.6 at.pct. Zn alloy sample, aged at 436°C for 17 days and 15 hr. (408 hr.).

The primary lamellae are resolved in Figures 18B (17.6 at.pct.Zn alloy sample, aged at 460°C for 25 hours) and 18C (22.16 at.pct.Zn alloy sample, aged at 520°C for 4 hr.).

Figure 19 (22.16 at.pct.Zn alloy aged at 520°C for 24 hrs.) exhibits a secondary reaction front. The front advances into the grain having the primary lamellae, almost perpendicular to the secondary lamellae. The secondary lamellae have a larger interlamellar spacing and are bulky, compared to the primary lamellae, which are thinner and have a smaller inter-lamellar spacing.

Among all the models for which the $D^{B}_{Zn}\delta$ values were calculated, they exhibit the best fit for the Petermann-Hornbogen model, in the $D^{B}_{Zn}\delta$ vs $\frac{1}{T}$ plot, for both alloys, in both primary and secondary precipitations. Also, this model showed consistency in the results, for small changes in

Figure 19 : Primary Lamellae

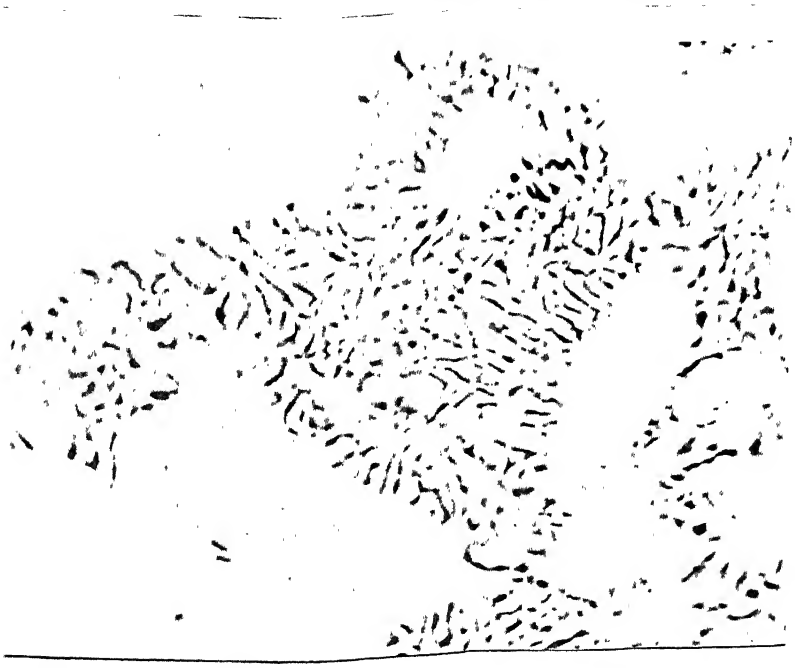

Fig.19A : 17.6 at.pct.Zn sample treated at 436°C for 17 days 21 hours (M = X)

Fig.19B : 17.6 at.pct.Zn treated at 460°C for 24 hours (M = 7(40X)

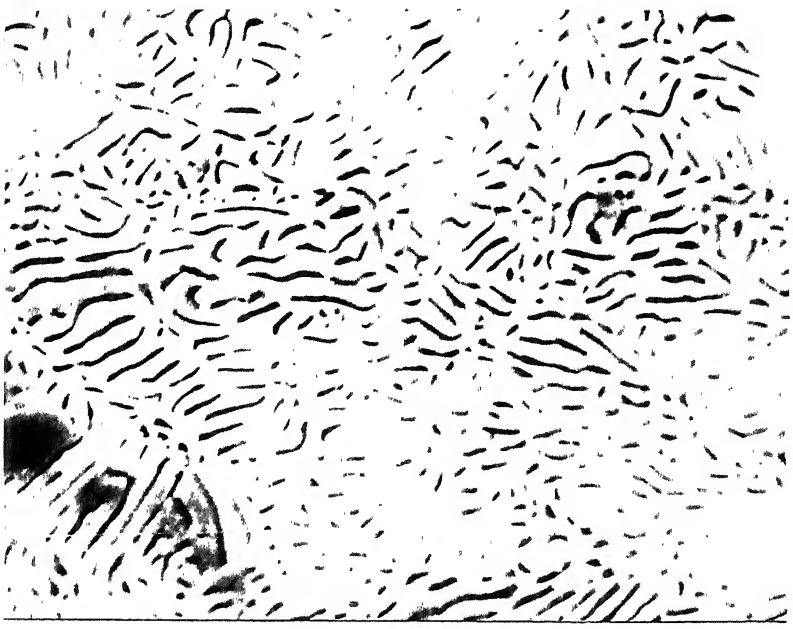

Fig.19C : 22.16 at.pct.Zn sample
treated at 520°C for
4 hours (M = [illegible] X)

Figure 19 : Secondary Reaction Front

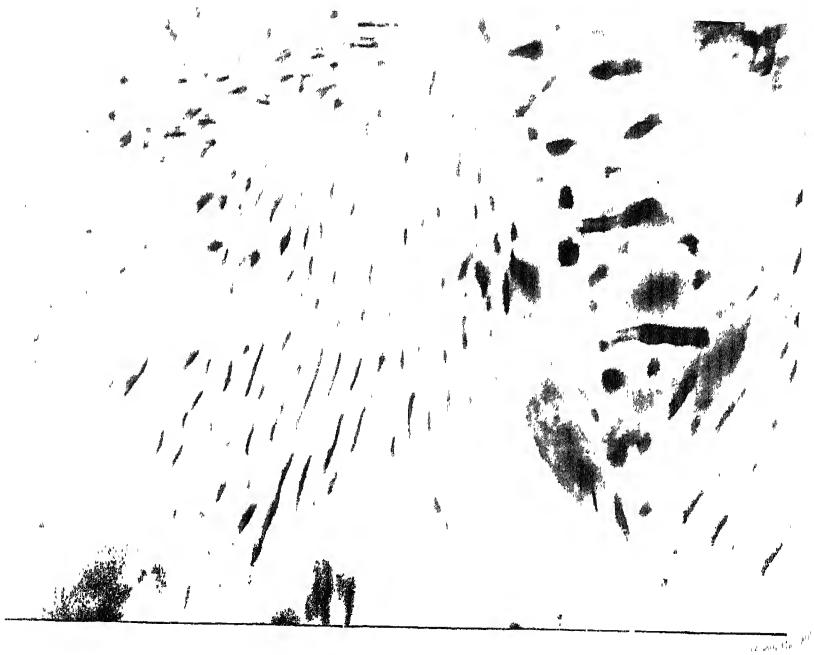

Fig.19 : 22.16 at.pct.Zn sample treated at 520°C for 24 hours (M = [illegible] X)

X_{Zn}^{α} or S values, whereas, such changes affected the results of other models drastically. These observations along with the consideration of chemical free energy change contribution to the driving force of secondary reaction indicate that the Petermann-Hornbogen model is the best suit among all the models investigated, for both primary and secondary precipitation in Fe + Zn alloys.

It has been observed that during the longer periods of aging, the secondary lamellae break-up into nodules. This could be explained on the following basis: the secondary lamellae are non-uniform in their thickness. The thicker regions grow at the cost of thinner regions, resulting in the breaking up of the lamellae into nodules. This is shown in Figures 10A,B,C, representing the 17.6 at.pct.Zn alloy specimen, treated at 487°C for 9 days.

Figure 20 : Instability of Lamellae during longer aging times

Fig.20A : 17.6 at.pct.Zn sample treated at 487°C for 216 hour (M= X)

Fig.20B : 17.6 at.pct.Zn sample treated at 487°C for 216 hours (M = X)

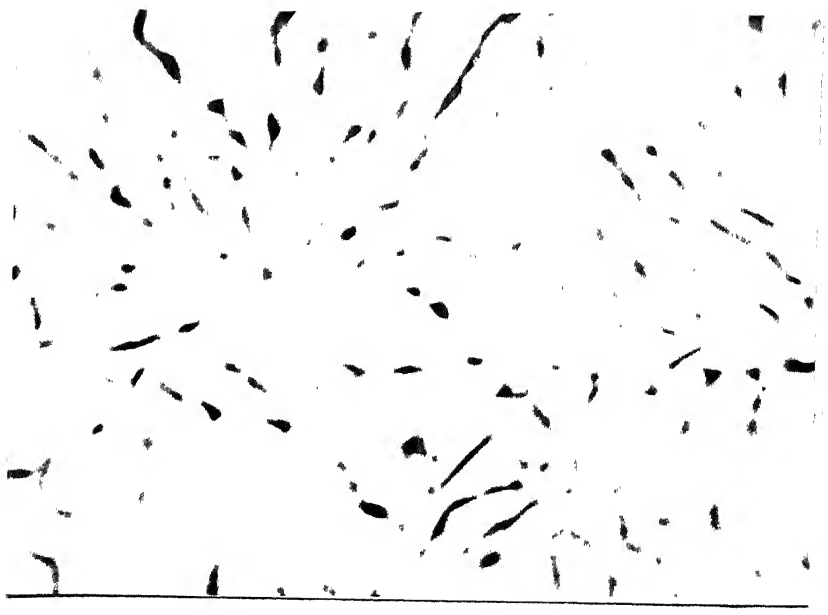

Fig.20 : 17.6 at.pct.Zn sample treated at 487°C for 216 hours (M = X)

CHAPTER 5

CONCLUSIONS

1. The discontinuous coarsening in Fe + Zn alloys was achieved by subjecting the specimens to longer times of aging at the aging temperatures selected for primary reaction itself. The coarsening process is found to be controlled by the migration of the reaction front.

2. Among all the models investigated, the Petermann-Hornbogen model happens to be the best suit for both the reactions. The Livingston-Cahn model does not describe the coarsening reaction completely, since it does not take into account, the chemical free energy available after the primary reaction.

3. The activation energy required for the primary and secondary reaction vary from 0.14 MJ/mole to 0.18 MJ/mole for different model. This falls in the range of activation energy required for diffusion of Zinc in Iron via the grain boundary.

4. The morphology of the discontinuous coarsening reaction characterizes that aging of the supersaturated α -Fe results in a lamellar aggregate of depleted α and Zn rich Γ, having a habit. The primary cells grow into other primary cells either at the original α -Fe grain boundaries or at primary cell intersections and secondary cells are nucleated.

5. The secondary cells, which are also lamellar aggregates of depleted α and Zn rich β, grow into the primary cells by decomposing them. These secondary cells have a larger interlamellar spacing, a slower growth rate and a larger volume fraction of β, than the primary cells from which they formed.

REFERENCES

1. Livingston and Cahn, Acta Met., 22, p.495, 1974.
2. C. Zenar, Trans. AMIE., 167, p.550, 1946.
3. R.A.Fournelle, Acta. Met., 27, p.1147, 1979.
4. Petermann and Hornbogen, Z. Metallk., 59, p.814, 1968.
5. K. Lucke, Z.Metallk., 52, p.1, 1961.
6. D. Turnbull, Acta. Met., 3, p.55, 1955.
7. Aaronson and Liu, Script. Met., 2, p.1, 1968.
8. J.W. Cahn, Acta. Met., 7, p.18, 1959.
9. G.R.Speich, Trans. AMIE, 242, p.1359, 1968.
10. Metals Handbook, ASM, 8, p.308, 1973.
11. E. Hornbogen, Met. Trans., 3, p.2717, 1972.
12. K.N. Tu, Met. Trans., 3, p.2769, 1972.
13. R.A.Fournelle and J.B. Clark, Met. Trans., 3, p.2757, 1972.
14. G.R. Speich, Trans. AIME, 227, p.754, 1963.
15. K.K.Rao, H. Herman, and L.E.Katz, Mat. Sci. Engg., 1, p.263, 1966.
16. H.I. Aaronson and J.B. Clark, Acta.Met., 16, p.845, 1968.
17. A.A. Keijzer, Ph.D. Thesis, Technische Hogeschool, Delft, Holland, 1970.
18. R.H. Hopkins and R.Kossowsky, Acta. Met., 19, p.203, 1971.
19. C.S. Smith, Trans. AIME, 45, p.533, 1953.
20. K.N. Tu and D. Turnbull, Acta. Met., 15, p.369, 1967.
21. R.A. Fournelle, Acta. Met., 27, p.1135, 1979.
22. M. Frebel, B. Predel, and U. Klisa, Z. Metallk., 65, p.311, 1974.

23. B. Predel and W. Gust, Met. Trans., A6, p.1237, 1974.

24. B.Predel and M.Frebel, Mat. Sci. Engg., 10, p.325, 1972.

25. D.B. Williams and J.W. Edington, Acta. Met., 24, p.323, 1976.

26. Hawkes, Johnson and Mehl, Trans. Am. Soc., Metals, 30, p.1049, 1942.

27. C. Haworth, H.A. Wriedt and J.A. Gula: June 1966, EC Bain Laboratory Publication, U.S. Steel Corporation.

Correction

Equation 14, modified by Aaronson and Liu has been re-written (i.e.) two more terms have been included in equation 14. The B_0', G, D_0 and B values have to be changed accordingly